AFRL-ML-WP-TR-2006-4202

COLLABORATIVE RESEARCH AND DEVELOPMENT CONTRACT
Delivery Order 0018: Grain-Structure Evolution During Thermomechanical Processing (TMP) of Superallloys

Jean-Philippe Thomas, Ph.D.

Universal Technology Corporation
1270 North Fairfield Road
Dayton, OH 45432-2600

MARCH 2006

Final Report for 01 September 2004 – 28 February 2006

Approved for public release; distribution unlimited.

STINFO COPY

MATERIALS AND MANUFACTURING DIRECTORATE
AIR FORCE RESEARCH LABORATORY
AIR FORCE MATERIEL COMMAND
WRIGHT-PATTERSON AFB, OH 45433-7750

NOTICE AND SIGNATURE PAGE

Using Government drawings, specifications, or other data included in this document for any purpose other than Government procurement does not in any way obligate the U.S. Government. The fact that the Government formulated or supplied the drawings, specifications, or other data does not license the holder or any other person or corporation; or convey any rights or permission to manufacture, use, or sell any patented invention that may relate to them.

This report was cleared for public release by the Air Force Research Laboratory Wright Site Public Affairs Office and is available to the general public, including foreign nationals. Copies may be obtained from the Defense Technical Information Center (DTIC) (http://www.dtic.mil).

AFRL-ML-WP-TR-2006-4202 HAS BEEN REVIEWED AND IS APPROVED FOR PUBLICATION IN ACCORDANCE WITH ASSIGNED DISTRIBUTION STATEMENT.

//signature//

RITA SCHOLES
Project Manager
Integration and Operations Division

//signature//

ROBERT ENGHAUSER
Acting Chief
Business Operations Branch
Integration and Operations Divsion

This report is published in the interest of scientific and technical information exchange, and its publication does not constitute the Government's approval or disapproval of its ideas or findings.

*Disseminated copies will show "//signature//" stamped or typed above the signature blocks.

REPORT DOCUMENTATION PAGE

Form Approved
OMB No. 0704-0188

1. REPORT DATE *(DD-MM-YY)*	2. REPORT TYPE	3. DATES COVERED *(From - To)*
March 2006	Final	09/01/2004 – 02/28/2006

4. TITLE AND SUBTITLE
COLLABORATIVE RESEARCH AND DEVELOPMENT CONTRACT
Delivery Order 0018: Grain-Structure Evolution During Thermomechanical Processing (TMP) of Superallloys

5a. CONTRACT NUMBER
F33615-03-D-5801-0018

5b. GRANT NUMBER

5c. PROGRAM ELEMENT NUMBER
62102F

6. AUTHOR(S)
Jean-Philippe Thomas, Ph.D.

5d. PROJECT NUMBER
4349

5e. TASK NUMBER
L0

5f. WORK UNIT NUMBER
4349L0VT

7. PERFORMING ORGANIZATION NAME(S) AND ADDRESS(ES)
Universal Technology Corporation
1270 North Fairfield Road
Dayton, OH 45432-2600

8. PERFORMING ORGANIZATION REPORT NUMBER
S-531-018

9. SPONSORING/MONITORING AGENCY NAME(S) AND ADDRESS(ES)
Materials and Manufacturing Directorate
Air Force Research Laboratory
Air Force Materiel Command
Wright-Patterson AFB, OH 45433-7750

10. SPONSORING/MONITORING AGENCY ACRONYM(S)
AFRL-ML-WP

11. SPONSORING/MONITORING AGENCY REPORT NUMBER(S)
AFRL-ML-WP-TR-2006-4202

12. DISTRIBUTION/AVAILABILITY STATEMENT
Approved for public release; distribution is unlimited. AFRL/WS PAO Case number AFRL/WS 06-2360, October 4, 2006.

13. SUPPLEMENTARY NOTES
Report contains color.

14. ABSTRACT
This research in support of the Air Force Research Laboratory, Materials and Manufacturing Directorate was conducted at Wright-Patterson AFB, Ohio from 1 September 2004 through 28 February 2006. Usual models of recrystallization are based on the Avrami formulation. They induce rigidities, mostly due to the lack of physic representativeness of parameters. A meso-scale mechanism-based model was developed. It is composed of two main parts that are a geometric framework and a set of equations which are to represent driving forces. The geometric framework is based on MesoStructure Units, which can be seen as aggregates of similar grains. It accepts two kinds of inputs, grain boundary velocities and nucleation rates, from which it is able to deduce the evolution of geometric variables of the microstructure. Driving forces equations are used to calculate these grain boundary velocities and nucleation rates through three groups of equations, which aim at representing the three stages of dynamic recrystallization: energy storage, nucleation, grain growth. Equations parameters have been identified so that the model fits the recrystallization behavior of ingot and wrought initial microstructures of Waspaloy.

15. SUBJECT TERMS
Recrystallization models, Grain microstructure, Superalloys

16. SECURITY CLASSIFICATION OF:			17. LIMITATION OF ABSTRACT:	18. NUMBER OF PAGES	19a. NAME OF RESPONSIBLE PERSON (Monitor)
a. REPORT	b. ABSTRACT	c. THIS PAGE			Rita Scholes
Unclassified	Unclassified	Unclassified	SAR	74	19b. TELEPHONE NUMBER *(Include Area Code)* (937) 656-6053

Standard Form 298 (Rev. 8-98)
Prescribed by ANSI Std. Z39-18

Introduction

Modeling tools for the prediction of microstructural evolution are needed to optimize thermomechanical processing, in order to guarantee consequent mechanical properties and reduce process definition time and manufacturing costs. The usual method, based on the so-called Avrami formulation, has been applied with great success for the past decades. In particular, its implementation in FEM codes subroutines, which require low additional computational power, has provided a useful tool for manufacturers [1]. However, this method exhibits some limitations. Firstly, when dealing for instance with nickel base superalloys, the presence of a precipitation domain at the low values of the hot working temperature range, may it be phase δ for niobium hardened ones as Superalloy 718, or γ' for titanium and aluminum hardened ones as Waspaloy, induces a change in recrystallization kinetics that can hardly be managed in another way than defining temperature intervals, at the limit of which the continuity of the model is not guaranteed [2]. In addition, subtle variations of composition for a given alloy from a manufacturer to another affect the solvus temperature of these phases, which should be accounted for by changing temperature interval limits. But since the Avrami formulation parameters are not physically representative, such changes are difficult to manage and the overall reliability of the model is affected. Secondly, the Avrami formulation is set for one-hit sequences of dynamic and metadynamic recrystallizations, whereas industrial process involves numerous steps from ingots to final products. In some cases, for one single processing step, as cogging, the total strain is reached by accumulating several hits, which produce successive waves of dynamic and metadynamic partial recrystallizations. To make the Avrami formulation deal with such cases requires the use of some modifications, which, once again, bring such a model into a questionable area of application. The third kind of limitation may be the most fundamental and stands as a long term problem. Both academic and industrial laboratories have been performing studies of microstructural evolution for numerous

alloys, which lead in the end to the development of Avrami models for many of them. But, even if the range of investigation is limited to nickel base superalloys only, there are far more alloys than what can be reasonably studied with extensive experiments over the full domains of temperature, strain rate, initial microstructure… etc. which are necessary to fit an Avrami model. Scientists and engineers have long identified similarities of behavior from an alloy to the other. But the use of the Avrami model prevents from connecting the studies. Whatever the amount of data that has been collected before on alloys of comparable compositions and exhibiting the same characteristics, it is not possible to benefit from a capitalization of this knowledge when it comes to develop a model of recrystallization based on the Avrami equation, because its parameters have limited physical meaning.

To progress in the direction of solving these limitations, it is necessary to develop a new kind of model of recrystallization. One of the difficulties lies in the fact that such a model has to satisfy at least the two following contradictory criteria:

- the model has to be physically-based, which means that its components and its adjustable parameters have to be as meaningful as possible,
- the model has to require relatively low computational power, not so much to insure that it is applicable with FEM calculations, but even before that, simply to be able to manage its resolution, since it requires far more time and analysis than running the model on FEM once it is ready for it.

A model that aims at being a good compromise of these criteria has been developed. It could be qualified as a meso-scale mechanism-based recrystallization model. It is positioned between, on the one hand, the low CPU power and low physics representation level of the “macro” Avrami model, and on the other hand, the high CPU power and high physics representation level of “micro” approaches like Monte-Carlo or

Cellular Automata. Inspired from previous models [3, 4], it was developed in the context of a program that aims at the development of models for microstructural evolution during the primary processing of superalloy ingots, firstly focused on Waspaloy [5].

In the first part of this paper, the method used to describe microstructures and their geometry-related properties will be presented. The second part deals with the representation of mechanisms of microstructural evolution, or in other words, the way driving forces affect microstructures described in the first part. The third part discusses the method used to carry out the resolution of the model so that it fits the behavior of Waspaloy, from primary processing of ingots to the forging of wrought microstructures.

I. Microstructure description – geometric framework

Any model of recrystallization relies on two complementary sides: the first is the set of assumptions used to describe microstructures, and the second is the set of equations that aim at representing driving forces. These two sides are connected through the integration method, by which these equations affect the modeled microstructures. The representation of mechanisms lies in this connection. For Avrami models for instance, even if they are integrated into the Avrami equation, these two sides can be identified originally. The microstructure description involves nuclei placed into a non-geometrically defined matrix, with possible impingement. And the driving forces are supposed to result in the nucleation and growth rates of nuclei. On the opposite, for Cellular Automata and Monte-Carlo models, the microstructure description involves a very refined regular grid and the (local) driving forces affect the behavior of cells. In the end, the aggregate of these cells is supposed to behave like grains, whose geometry is not actually defined.

The microstructure description used in this model is located between these two extremes. It is based on Meso-Structural Units (MSUs). These can be understood as families of grains that have similar properties, may it be due to intrinsic parameters (e.g. specific crystallographic orientation) or because they had similar previous histories. These grains are expected to exhibit similar behaviors during further evolution. Grains are assigned two kinds of variables to define them. For geometric description, these variables are the grain density and at least one dimension. Few others are added to define more intrinsic properties such as Taylor factor or dislocation density. Grains and MSUs properties are supposed to be averages over the population they represent. Such description based on MSUs aims at lightening computational power. It allows distinction between grains that are expected to have different evolutions, but without going as far as describing each grain individually. For instance, to represent the microstructure of an alloy that is recrystallizing, at least two MSUs are

required: one for initial grains, and one for the recrystallized ones, the second being consuming the first. But if specific insight is wished, more MSUs can be defined. For example, another one will be needed to distinguish between recrystallized grains that appeared during the current deformation and those that appeared during previous hits. The latter are expected to be coarser and have higher dislocation densities than the ones of the current hit.

To deal with the part of the microstructure description that is only related to geometry, the model relies on what can be called a geometric framework, more than just a geometric description. It means that the geometric aspects do not only lie in variables, but also in geometric laws that connect them. For instance, in the model, a grain is defined as much by its dimensions as by the equation used to calculate its boundary surface. This is related to the language used to implement the model, C++, object-oriented, in which classes of objects are not only defined by "member variables" but also by "member functions". The transition from a simple geometric description to a geometric framework is about the same as from a C structure to a C++ class. The role of the functions that are attached to the geometric description is to provide a clear set of rules to constrain the various geometric variables in a framework, in order to insure that these variables remain meaningful altogether and that the geometric part of the model is somewhat autonomous and self-consistent. The most critical operation for geometric representativeness and consistency is the calculation of grain interactions, as it combines all geometric assumptions.

Two types of grain interactions have to be considered:

- *Interactions between grains of the same MSU:* These imply no change of the volume of the MSU. As a consequence, any change of grain size (or equivalently of boundary density) has to be accompanied by a change of the grain density.

This is typically the case of static grain growth, where the finest grains of the microstructure disappear *via* grain boundary tension.

- *Interactions between grains of different MSUs:* These imply a change of the volume of the MSU, as the grains of the MSU grow or decrease keeping a constant grain density. In order to insure the volume conservation of the whole structure, the volume variation of an MSU due to its interaction with grains of another MSU has to be compensated by an opposed variation of the volume of the second one.

I.A.Isotropic grains interactions

In the case of isotropic grains, for any MSU i, grains are supposed to be spheres of diameter D_i. Their volume density is noted n_i. The volume enclosed in the grain envelope is expressed in equation (I-1) and the total volume of MSU i is given by equation (I-2).

$$v_{ei} = \frac{\pi}{6} D_i^3 \tag{I-1}$$

$$V_{ei} = n_i v_{ei} = n_i \frac{\pi}{6} D_i^3 \tag{I-2}$$

Grain boundary surfaces will be needed too. The surface s_{ei} of one grain is given by equation (I-3) and the boundary density of MSU i, noted S_{ei}, is given by equation (I-4).

$$s_{ei} = \pi D_i^2 \tag{I-3}$$

$$S_{ei} = \frac{n_i s_{ei}}{2V_{ei}} = \frac{3}{D_i} \tag{I-4}$$

The volume variation of grains is related to the volume swept by its migrating grain boundary, as expressed in equation (I-5), where $\dot{u}$ is the migration rate of a boundary of surface s.

$$\dot{v} = s\dot{u} \tag{I-5}$$

For the variation of the volume defined by a sphere, equation (I-5) is naturally verified, as revealed by the derivation of equation (I-1), shown below in equation (I-6), where $\dot{u}_i$ is the average migration rate of the boundary of grains i.

$$\dot{v}_{ei} = \pi D_i^2 \frac{\dot{D}_i}{2} = s_{ei}\dot{u}_i \tag{I-6}$$

I.A.1. Interaction probabilities for isotropic "necklace" topology

In order to calculate the interaction of the grains of MSU i with another MSU j, it is necessary to decompose equation (I-6) by identifying the contribution of each MSU of the structure. The decomposition of equation (I-6), in the sum of equation (I-7), allows the distinction of the various contributions. In the latter equation, s_{ij} can be seen as the statistical expectancy of the surface of contact of a grain of MSU i with grains of MSU j, $\dot{u}_{ij}$ is the migration rate of a grain i – grain j boundary, and $\dot{v}_{ij}$ is the volume variation of a grain i due to its interaction with grains of MSU j.

$$\dot{v}_{ei} = \sum_{j=0}^{N_{MSU}-1} s_{ij}\dot{u}_{ij} = \sum_{j=0}^{N_{MSU}-1} \dot{v}_{ij} \tag{I-7}$$

Assuming a uniform probability of contact with grains of any MSU j (through their boundary) among all the grains of the microstructure, one can write equations (I-8) and (I-9).

$$s_{ij} = q_j s_{ei} \tag{I-8}$$

where the probability of contact q_j is :

$$q_j = \frac{n_j s_{ej}}{\sum_{k=0}^{N_{MSU}-1} n_k s_{ek}} = \frac{n_j s_{ej}}{S_{total}} \tag{I-9}$$

This probability of interaction is consistent with previous models [3] and has even been used explicitly elsewhere too [6, 4].

Then the volume variation of a grain of MSU i due to its interaction with grains of MSU j is given by equation (I-10).

$$\dot{v}_{ij} = s_{ij}\dot{u}_{ij} = s_{ei}\frac{n_j s_{ej}}{S_{total}}\dot{u}_{ij} \qquad \text{(I-10)}$$

And the volume variation of the whole MSU i due to its interaction with MSU j is expressed in equation (I-11).

$$\dot{V}_{ij} = n_i s_{ij}\dot{u}_{ij} = n_i s_{ei}\frac{n_j s_{ej}}{S_{total}}\dot{u}_{ij} = -n_j s_{ej}\frac{n_i s_{ei}}{S_{total}}\dot{u}_{ji} = -n_j s_{ji}\dot{u}_{ji} = -\dot{V}_{ji} \qquad \text{(I-11)}$$

Hence volume conservation of the whole microstructure is insured.

This approach is valid as long as the various grains only interact through their envelope. However, volume nucleation has been observed, on Waspaloy ingot microstructures for instance [5]. In such a case, the previous assumptions are not acceptable anymore, since the surface of contact between grains of different MSUs does not only lie in their envelope but also in the interface between the grain matrix and the bubbles of recrystallized grains that nucleated and subsequently grew *inside* the volume of initial grains. Therefore, preceding equations have to be modified to account for a "necklace and bubbles" topology.

I.A.2. Interaction probabilities for isotropic "necklace and bubbles" topology

In this new topology, bubbles of grains are allowed to develop inside the grains of MSU i. The first modification to bring to the model relates to the volume of grains. It is necessary to accept to give up the rather comfortable equation connecting the volume of grains to their diameter. From now, v_{ei}, in equation (I-1), only symbolizes the volume enclosed in the grain envelope, but not the volume of material that really belongs to the grain itself. The latter will be noted v_i, and it is inferior or equal to v_{ei}. v_i is an additional

constitutive parameter of the grains of MSU i to be considered on the same level as their diameter D_i in terms of geometric description. This parameter will allow dealing with bubbles topology in a realistic and physically admissible way. Firstly, one can define naturally the fraction X_{bi} of bubbles in the grains of MSU i as given by equation (I-12).

$$X_{bi} = 1 - \frac{v_i}{v_{ei}} \tag{I-12}$$

A material parameter is needed for an accurate definition of the microstructure: the density of sites of volume nucleation, noted n_{PSN}. Typically, it will be the density of second phase particles that induce a wide-enough spread of crystallographic orientations in their neighborhood to activate nucleation [7]. Using this parameter makes possible to calculate the diameter D_{bi} of the bubbles in the grains of MSU i, thanks to equation (I-14), which is deduced from equation (I-13).

The volume of bubbles in a grain i is :

$$n_{PSN} v_{ei} \frac{\pi}{6} D_{bi}^3 = v_{ei} - v_i \tag{I-13}$$

Then

$$D_{bi} = \left(\frac{6 X_{bi}}{\pi n_{PSN}} \right)^{1/3} \tag{I-14}$$

I.A.2.a. Surface of interaction of bubbles

In order to evaluate grain interaction probabilities later, the surface of contact of the bubbles with the matrix of a grain has to be calculated. It is not simply the sum of the surfaces of the bubbles written in equation (I-15), because some impingement of bubbles may occur when they are large enough.

$$s_{bei} = v_{ei} n_{PSN} \pi D_{bi}^2 \tag{I-15}$$

Equation (I-5) can be applied to the volume variation of the bubbles, which gives $\dot{v}_{bi}$ in equation (I-16), where s_{bmi} is the surface of contact between a bubble and the surrounding matrix of MSU i, and q_{bmi} is the fraction of the bubble surface (πD_{bi}^2) that is in contact with the matrix but not with another bubble. $\dot{u}_{bmi}$ is the migration rate of bubble-matrix interface.

$$\dot{v}_{bi} = s_{bmi}\dot{u}_{bmi} = q_{bmi}\pi D_{bi}^2\dot{u}_{bmi} \tag{I-16}$$

Then

$$\dot{X}_{bi} = q_{bmi}s_{bei}\dot{u}_{bmi} \tag{I-17}$$

In equation (I-17), $s_{bei}\dot{u}_{bmi}$ would be the volume variation of bubbles if there were no impingement, i.e. if the volume consumed were only in the matrix. But, statistically, only a fraction 1-X_{bi} of this volume variation would be taken over the matrix. The complement of this fraction would be taken only virtually over neighboring bubbles as they impinge. Equation (I-18) comes as a consequence.

$$q_{bmi} = 1 - X_{bi} \tag{I-18}$$

And therefore, the fraction of surface of the envelope of bubbles that is involved in impingement is equal to the volume fraction of bubbles X_{bi}. Finally, the surface s_{bi} of the bubbles that is really in contact with the matrix of a grain of MSU i, is given by equation (I-19).

$$s_{bi} = q_{bmi}s_{bei} = (1 - X_{bi})v_{ei}n_{PSN}\pi D_{bi}^2 = v_i\, n_{PSN}\pi D_{bi}^2 \tag{I-19}$$

Knowing the actual surface of interaction of bubbles of recrystallized grains with the surrounding grain matrix, it is possible to investigate the various types of grain interactions and their respective contributions.

I.A.2.b. Total grain boundary surfaces

Not all grains are subjected to volume nucleation. In practice, only the biggest ones can exhibit a bubble topology. For finer grains too, nucleation can be enhanced by second phase particles, but bubbles are quickly connected to the developing necklaces, and the influence of a bubble topology can be neglected. As a consequence, support for bubble topology is only activated for the first N_{bt} MSUs of the structure, as they may be initialized with coarse ingot grains. N_{bt} is strictly lower than N_{MSU}, which means that at least the current recrystallized grains, which are stored in the MSU of highest index, are supposed not to be a place for volume nucleation. Recrystallized grains are finer by definition. In addition, in order to limit complexity, assumption is made that the only grains that can be found in bubbles are those which index is higher than N_{bt}. In other words, bubbles inside of bubbles, like Russian headstocks, are not allowed. This is not really a restriction. Typically, the MSUs of which index is between N_{bt} and the highest index, will contain grains that recrystallized during the previous steps of the process or during previous hits. Thus one can expect that they will not be coarse enough to develop a bubble topology anyway.

As seen previously, in equation (I-9), the calculation of probabilities of contact with the grains of another MSU j involves the fraction of the grain boundary surface of this MSU among the total boundary surface. The situation here is a little bit more complex since two fundamentally different types of grain interactions exist. Envelope-envelope interactions (Figure I-1-a) and bubble-envelope interactions (Figure I-1-b) do not have the same effects. The first affect grain size and volume, whereas the second only affect the volume of grains from the inside, without changing their envelope dimension. One could think about bubble-bubble interactions here but contact between bubbles has already been accounted for at the occasion of previous bubbles impingement considerations.

As a consequence, it is necessary to distinguish two total surfaces: on the one hand, the total boundary surface involved in envelope-envelope interactions, and on the other hand, the total boundary surface involved in bubble-envelope interactions. They are noted respectively $S_{e\,total}$ and $S_{b\,total}$. The latter comes naturally, in equation (I-20).

$$S_{b\,total} = \sum_{k=0}^{N_{bt}-1} n_k s_{bk} \tag{I-20}$$

The total surface of grain boundaries involved in envelope-envelope interactions, $S_{e\,total}$, is the total surface of grain envelopes minus the part of envelope boundaries that are also bubble boundaries, which is $S_{b\,total}$ by definition. This is mathematically translated in equation (I-21).

$$S_{e\,total} = \sum_{k=0}^{N_{MSU}-1} n_k s_{ek} - S_{b\,total} \tag{I-21}$$

Knowing these two total boundary surfaces, normalization of grain interaction probabilities will be possible.

I.A.2.c. Grain boundary surfaces involved in each type of interaction

As a distinction was made between envelope-envelope and bubble-envelope total boundary surfaces, the same has to be carried out for individual grain boundary surfaces. For the grains of each MSU i, parameters q_{eei} and q_{bei} are defined as the fraction of the boundary surface of their envelope being in contact with respectively the envelope boundary of other grains or with the bubble boundary of other grains. For i strictly lower than N_{bt}, q_{bei} is null, as these grains are not allowed to be in the bubbles of other grains. And consequently, q_{eei} is equal to 1. For other MSUs ($i \geq N_{bt}$), assumption is made that each of them contributes to $S_{b\,total}$ proportionally to its own surface, which is expressed in equation (I-23), from which q_{bei} is deduced in equation (I-24). Equation

(I-22) defines an intermediate value, $S_{ebc\ total}$, as the total amount of envelope boundaries of grains that can have nucleated in bubbles, and thus which potentially contribute to the bubbles surface. Finally, q_{eei} is the complementary part of q_{bei}, as written in equation (I-25).

$$S_{ebc\ total} = \sum_{k=N_{bt}}^{N_{MSU}-1} n_k s_{ek} \tag{I-22}$$

$$q_{bei}\, n_i\, s_{ei} = \frac{n_i\, s_{ei}}{S_{ebc\ total}} S_{b\ total} \tag{I-23}$$

Then

$$q_{bei\ \ i \geq Nbt} = \frac{S_{b\ total}}{S_{ebc\ total}} \tag{I-24}$$

$$q_{eei} = 1 - q_{bei} \tag{I-25}$$

Equation (I-24) shows that all the MSUs which envelope contributes to interaction in bubbles have the same proportion of envelope-envelope and envelope-bubble interactions.

It is now possible to evaluate the probability of interaction for each pair of MSUs.

I.A.2.d. Interaction probabilities

We investigate now the probability for a surface unit of grain boundary of MSU i to be an interface with a grain of MSU j. In other words, we are looking for the equivalent of equation (I-9) but for the case of a necklace and bubbles topology. Here again, the distinction between envelope-envelope interactions and envelope-bubble interactions is necessary. Thus we define two parameters, q_{eeij} and q_{beij}, as the probabilities of contact involving respectively envelope-envelope and envelope-bubble interactions.

The first probability, q_{eeij}, is the fraction of the envelope surface of grain i that is in contact with other grain envelope (q_{eei}), multiplied by the fraction (q_{eej}) of the surface of

envelope of grains of MSU j ($n_j\ s_{ej}$) which is also in contact with a grain envelope, among all envelope boundaries ($S_{e\ total}$). This is written in equation (I-26).

$$q_{eeij} = q_{eei}\frac{q_{eej}\ n_j s_{ej}}{S_{e\ total}} \tag{I-26}$$

The expression of q_{beij} depends on the value of i. If i is strictly lower than N_{bt}, then q_{beij} is the fraction of the bubble surface of a grain of MSU i (q_{bej}) that is in contact with the envelope of grains of MSU j ($n_j s_{ej}$), among all bubble boundaries ($S_{b\ total}$). This is expressed by equation (I-27).

$$q_{beij\ i<Nbt} = \frac{q_{bej}\ n_j s_{ej}}{S_{b\ total}} \tag{I-27}$$

If i is higher than or equal to N_{bt}, q_{beij} is the fraction of the envelope surface of grain i (q_{bei}) that can be also a bubble boundary, multiplied by the surface of bubbles inside grains of MSU j ($n_j s_{bj}$), among all bubble boundaries ($S_{b\ total}$). This is translated in equation (I-28).

$$q_{beij\ i\geq Nbt} = q_{bei}\frac{n_j s_{bj}}{S_{b\ total}} \tag{I-28}$$

Using these probabilities, it is possible to evaluate the variations of grain size, grain volume and total MSU volume in the various possible situations.

I.A.2.e. Variations of grain size, grain volume and whole MSU volume

Variations of grain size, grain volume and MSU volume depend on the interaction type, that is if, on the one hand, it is an envelope-envelope interaction or an envelope-bubble one, and on the other hand, if it is an interaction between grains of different MSUs or of the same MSU.

Interactions between grains of different MSUs

Interactions between different MSUs are the most various but also the easiest to deal with. The first, which is envelope-envelope interaction, affects all parameters, as written in equations (I-29), (I-30) and (I-31).

$$\dot{v}_{ij} = q_{eeij}\, s_{ei}\, \dot{u}_{ij} \tag{I-29}$$

$$\dot{V}_{ij} = n_i\, \dot{v}_{ij} \tag{I-30}$$

$$\dot{D}_{ij} = 2 q_{eeij}\, \dot{u}_{ij} \tag{I-31}$$

The second, which is envelope-bubble interaction, involve actually two symmetrical behaviors, depending on the location of grains. If we assume that i is lower than N_{bt} and j is higher than N_{bt}, then grains i contain some j grains. For the first ones, there will only be a volume variation of the grains and of the MSU, but not of the apparent grain size. For the others, all parameters will change. These behaviors are written in equations (I-32) to (I-37). Equation (I-36) is developed to demonstrate that envelope-bubble interactions, though built by following a somewhat complex process, are finally volume conservative too.

$$\dot{v}_{ij} = q_{beij}\, s_{bi}\, \dot{u}_{ij} \tag{I-32}$$

$$\dot{V}_{ij} = n_i\, \dot{v}_{ij} \tag{I-33}$$

$$\dot{D}_{ij} = 0 \tag{I-34}$$

And inversely,

$$\dot{v}_{ji} = q_{beji}\, s_{ej}\, \dot{u}_{ji} \tag{I-35}$$

$$\dot{V}_{ji} = n_j \dot{v}_{ji} = q_{beji} n_j s_{ej} \dot{u}_{ji} = -q_{bej} \frac{n_i s_{bi}}{S_{btotal}} n_j s_{ej} \dot{u}_{ij}$$
$$= -n_i \frac{q_{bej} n_j s_{ej}}{S_{btotal}} s_{bi} \dot{u}_{ij} = -n_i q_{beij} s_{bi} \dot{u}_{ij} = -\dot{V}_{ij} \quad \text{(I-36)}$$

$$\dot{D}_{ji} = 2 q_{beji} \dot{u}_{ji} \quad \text{(I-37)}$$

Interactions between grains of the same MSU

Interactions between grains of the same MSU involve envelope-envelope interactions only. They produce no change of the total volume of the MSU, but an increase of the volume and size of grains. Consequently, in order to keep MSU volume constant, grain density has to decrease.

Equivalence between grain boundary density and grain size is written in equation (I-38). This equation is derived in equation (I-39). The variation of all parameters comes from the boundary density that disappears due to boundary migration, whose effect is written in equations (I-40) and (I-41). It can be understood as the fact that some moving boundaries meet each other and only one boundary remains where there were two. Finally, comparing equations (I-39) and (I-41) gives the relationship between the boundary migration rate and the grain size variation.

On the one hand $$S_{ei} = \frac{n_i s_{ei}}{2V_i} = \frac{3}{(1-X_{bi})D_i} \quad \text{(I-38)}$$

Then, by derivation, as X_{bi} does not change through in-MSU interactions:

$$\dot{S}_{ei} = -\frac{3\dot{D}_i}{(1-X_{bi})D_i^2} \quad \text{(I-39)}$$

On the other hand $$\dot{v}_{swept\,i} = (1-X_{bi}) S_{ei} q_{eeii} \dot{u}_{ii} \quad \text{(I-40)}$$

$$\dot{S}_{ei}^{-} = S_{ei} \dot{v}_{swept\,i} = (1-X_{bi}) S_{ei}^2 q_{eeii} \dot{u}_{ii} = \frac{9}{(1-X_{bi})D_i^2} q_{eeii} \dot{u}_{ii} \quad \text{(I-41)}$$

Combination of (I-39) and (I-41) gives:

$$\dot{D}_i = 3q_{eeii}\dot{u}_{ii} \tag{I-42}$$

Once the grain size variation is obtained, it has to be translated into the grain volume variation. By definition of X_{bi}, one can write equation (I-43). As X_{bi} does not change through in-MSU interactions, the derivation of the latter leads to equations (I-44) and then (I-45).

$$1 - X_{bi} = \frac{v_i}{v_{ei}} = \frac{v_i}{\frac{\pi}{6}D_i^3} \tag{I-43}$$

$$\dot{v}_i \ \frac{\pi}{6}D_i^3 = v_i \ \frac{\pi}{2}D_i^2\dot{D}_i \tag{I-44}$$

$$\frac{\dot{v}_i}{v_i} = \frac{3\dot{D}_i}{D_i} = (1 - X_{bi})S_{ei}\dot{D}_i \tag{I-45}$$

Another refinement is still needed to be able to represent correctly ingot microstructure geometry: the grains of ingot microstructures are anisotropic. For them, the assumption used until now that grains can be represented by spheres is not appropriate.

I.B. Anisotropic grains

To deal with the evolution of anisotropic structures, as solidification ones, which exhibit columnar grains, it can be interesting to investigate an extension of the spherical grains behavior formulation to an ellipsoidal configuration. Actually, it does not come as naturally as one could expect.

For an MSU i, grains are now described as ellipsoids of main axis D_{xi}, D_{yi}, D_{zi}. Their volume density is still noted n_i. The volume defined by the grain envelope is expressed in equation (I-46) and the total volume of MSU i is given by equation (I-47) below.

$$v_{ei} = \frac{\pi}{6}D_{xi}D_{yi}D_{zi} \tag{I-46}$$

$$V_{ei} = n_i \, v_{ei} = n_i \, \frac{\pi}{6} D_{xi} D_{yi} D_{zi} \tag{I-47}$$

When it comes to evaluate the surface of an ellipsoidal grain boundary, there is actually a problem: no general analytical equation for the surface of a three-axis ellipsoid exists. Only for two-axis ellipsoids, two equations exist depending on the shape of the ellipsoid, *i.e.* if the original sphere has undergone uniaxial compression or uniaxial traction. However, applying equation (I-5) to the derivative of equation (I-46), shown in equation (I-48) (considering that the migration rate is the same on each of the three axis) gives a way out to define the grain boundary surface, shown in equation (I-49).

$$\dot{v}_{ei} = \frac{\pi}{3}\left(D_{xi} D_{yi} + D_{yi} D_{zi} + D_{zi} D_{xi}\right)\frac{\dot{D}_i}{2} = \frac{\pi}{3}\left(D_{xi} D_{yi} + D_{yi} D_{zi} + D_{zi} D_{xi}\right)\dot{u}_i \tag{I-48}$$

$$s_{ei} = \frac{\pi}{3}\left(D_{xi} D_{yi} + D_{yi} D_{zi} + D_{zi} D_{xi}\right) \tag{I-49}$$

The latter is different from any equation giving the surface of an ellipsoid. The reason for that lies in the fact that when the link is made between equations (I-5) and (I-48), assumption is implicitly made that when an ellipsoid grows or decreases through the migration of its boundary, orthogonally to its boundary, due to a pressure, it remains an ellipsoid. This assumption is wrong. This lies in the difference between the real surface that should be applied in equation (I-5) and the one given by equation (I-49). This difference can be up to 30%, but it is already a noticeable improvement compared to considering grains as spheres. In addition, these surface considerations should be seen more as a way to access problems of space filling that derive into probabilities of contacts of grains, than actual grain surfaces anyway.

Most of the equations of the isotropic case do not really depend on the grain shape because their expressions only involve boundary surfaces. Thus from that point, all the previous equations related to interactions between grains of different MSUs (interaction probability, volume variations, grain size variations etc.) can be applied directly to

anisotropic grains, just taking care to apply the appropriate surface expressions. One can see here one of the advantages of defining properly a geometric framework.

However, for interactions between grains of the same MSU, some equations need few modifications to be applied correctly, because the grain boundary density, given by equation (I-50), is different from its isotropic form.

$$S_{ei} = \frac{n_i s_{ei}}{2V_i} = \frac{1}{1-X_{bi}}\left(\frac{1}{D_{xi}} + \frac{1}{D_{yi}} + \frac{1}{D_{zi}}\right) \tag{I-50}$$

Derivation of the latter, assuming the variation of dimensions is the same on all axis, gives equation (I-51).

$$\dot{S}_{ei} = -\frac{\dot{D}_i}{(1-X_{bi})}\left(\frac{1}{D_{xi}^2} + \frac{1}{D_{yi}^2} + \frac{1}{D_{zi}^2}\right) \tag{I-51}$$

The volume swept by the moving boundaries written in equation (I-52) is still as written previously in equation (I-40). It leads however to a new expression for the diminution of boundary density in equation (I-53). The combination of equations (I-51) and (I-53) gives the grain size variation, written in equation (I-54).

$$\dot{v}_{swept\,i} = (1-X_{bi}) S_{ei}\, q_{eeii}\, \dot{u}_{ii} \tag{I-52}$$

and $$\dot{S}_{ei}^{-} = S_{ei}\,\dot{v}_{swept\,i} = (1-X_{bi}) S_{ei}^2\, q_{eeii}\, \dot{u}_{ii} = \frac{1}{(1-X_{bi})}\left(\frac{1}{D_{xi}} + \frac{1}{D_{yi}} + \frac{1}{D_{zi}}\right)^2 q_{eeii}\, \dot{u}_{ii} \tag{I-53}$$

Then $$\dot{D}_i = \frac{\left(\frac{1}{D_{xi}} + \frac{1}{D_{yi}} + \frac{1}{D_{zi}}\right)^2}{\frac{1}{D_{xi}^2} + \frac{1}{D_{yi}^2} + \frac{1}{D_{zi}^2}} q_{eeii}\, \dot{u}_{ii} \tag{I-54}$$

Once the grain size variation is obtained, it has to be translated into the grain volume variation. By definition of X_{bi}, one can write equation (I-55).

$$1 - X_{bi} = \frac{v_i}{v_{ei}} = \frac{v_i}{\frac{\pi}{6} D_{xi} D_{yi} D_{zi}} \tag{I-55}$$

As X_{bi} does not change through in-MSU interactions, the derivation of the latter leads to equations (I-56) and (I-57).

$$\dot{v}_i \frac{\pi}{6} D_{xi} D_{yi} D_{zi} = v_i \frac{\pi}{6} \left(D_{xi} D_{yi} + D_{yi} D_{zi} + D_{zi} D_{xi} \right) \dot{D}_i \tag{I-56}$$

then

$$\frac{\dot{v}_i}{v_i} = \dot{D}_i \left(\frac{1}{D_{xi}} + \frac{1}{D_{yi}} + \frac{1}{D_{zi}} \right) = (1 - X_{bi}) S_{ei} \dot{D}_i \tag{I-57}$$

The comparison of the last equation with equation (I-45) reveals that its latest form is the one to use to make it independent of grain shape assumptions and finally come back into the geometric framework.

I.C. Geometric effects of nucleation on grains and MSUs

To initiate significant grain interactions, the MSU that contains the recrystallized grains has to be initialized and renewed thanks to the reception of nuclei coming form other MSUs, and progressively during deformation, more and more from itself. It means that some volume of initial grains has to be transferred to the MSU of recrystallized grains. Such transfer affects all geometric variables.

Two nucleation rates for each MSU are defined. The first, usual one, which is responsible for necklace formation is noted $\dot{n}_{N\,i}$. The second, more unusual, is the nucleation rate in the volume, noted $\dot{n}_{NV\,i}$. Nuclei size is supposed to be the same in any MSU and noted $D_{N.}$ When nuclei are generated in an MSU, it is responsible for two volume losses for the MSU and its grains, depending on the site of nucleation considered. Equations (I-58) and (I-59) show the volume variations due to necklace nucleation. Equations (I-60) and (I-61) are almost identical for volume nucleation.

$$\dot{v}_{Ni} = \dot{n}_{Ni} \frac{\pi}{6} D_N^3 \tag{I-58}$$

$$\dot{V}_{Ni} = n_i \dot{v}_{Ni} = n_i \dot{n}_{Ni} \frac{\pi}{6} D_N^3 \tag{I-59}$$

$$\dot{v}_{NVi} = \dot{n}_{NVi} \frac{\pi}{6} D_N^3 \tag{I-60}$$

$$\dot{V}_{NVi} = n_i \dot{v}_{NVi} = n_i \dot{n}_{NVi} \frac{\pi}{6} D_N^3 \tag{I-61}$$

When it comes to evaluate the effect of nucleation on grain size, only necklace nucleation affects the envelope of grains and thus their dimensions. To convert the volume variation of equation (I-58) into a grain dimension variation, once again, equation (I-5) is applied. Even if the envelope boundary may not actually migrate, it moves on a geometric point of view, and the relationship between volume change and boundary movement remains identical. Equation (I-62) comes as a result of the inversion of equation (I-5) applied in this context.

$$\dot{D}_{Ni} = 2 \frac{\dot{v}_{Ni}}{s_{ei}} \tag{I-62}$$

It is to be noticed that the growth of bubbles due to volume nucleation comes naturally through the geometric framework. As soon as volume nucleation is initiated, the diminution of the volume of material that belongs to the grain is greater than the volume delimited by its envelope, because equation (I-62) is only applied for necklace nucleation. The consequence of such volume diminution is an increase of the fraction of bubble in equation (I-12), which induces an increase of the bubble diameter in equation (I-14). Then the chain of consequences continues with an increase of the surface of interaction of bubbles in equation (I-19), which affects further all the probabilities of grains interactions. The overall probability and surface of interaction of recrystallized grains with initial grains increases, which is to produce an acceleration of the

consumption of initial grains by the recrystallized ones, just by geometric effects. If the same density of nuclei were entirely affected to the necklace, recrystallized grains would have lower surface of interaction with initial grains, which would lead to a lower contribution of grain growth to the recrystallization rate.

To finish with nucleation, the transfer of nuclei to the MSU of recrystallized grains has to be dealt with. First, the total volume of nuclei produced in the other MSUs has to be added in order to know the volume increase of the MSU of recrystallized grains, whose index is supposed to be N_{MSU} - *1*. This volume is evaluated using equation (I-63).

$$\dot{V}_N = \sum_{i=0}^{N_{MSU}-2} \dot{V}_{N\,i} + \dot{V}_{NV\,i} \tag{I-63}$$

This volume variation is added to the volume variations that are due to grain interactions. To evaluate the grain size variation induced by the nuclei that are added to the MSU (a grain refinement one can expect), it is accounted in a way similar to the interaction of an MSU with itself. But instead of considering a grain boundary density diminution through a swept volume, the reception of nuclei is treated as an increase of the boundary density. As a consequence, the total surface of nuclei generated in the structure is needed, including those that appeared in the MSU of recrystallized grains itself. It has to be normalized by the volume of the MSU of recrystallized grains to be converted into its local grain boundary density increase. This is calculated using equation (I-64).

$$\dot{S}_N = \frac{\pi D_N^2}{V_{N_{MSU}-1}} \sum_{i=0}^{N_{MSU}-1} \dot{n}_{N\,i} + \dot{n}_{NV\,i} \tag{I-64}$$

We have to precise that during the numerical integration of the model, it is always the new volume $V_{N_{MSU}-1}(t+\delta t)$ that is used when some nucleation occurs, in order to avoid any division by a null term. By the way, this allows in addition dealing properly with the initialization of the MSU of recrystallized grains, when it receives the first nuclei.

Using equation (I-51) for the case of isotropic grains and without bubbles gives the grain size variation of the recrystallized grains that is related to nucleation. It is written in equation (I-65).

$$\dot{D}_N = -\frac{\dot{S}_N \, D^2_{N_{MSU}-1}}{3} = -\frac{3\dot{S}_N}{S^2_{e\,N_{MSU}-1}} \tag{I-65}$$

The second form of the expression is the actual one used. And when the MSU of recrystallized grains has not been initialized yet, the boundary density that is used to avoid a division by a null term is the one resulting from the integration of the nuclei boundary generation through the increment: $\dot{S}_N \, \delta t$.

Restricting equation (I-57) to the case of isotropic grains that contain no bubble, gives the apparent volume variation of the grains, in equation (I-66).

$$\frac{\dot{v}_N}{v_{N_{MSU}-1}} = S_{e\,N_{MSU}-1} \, \dot{D}_N \tag{I-66}$$

As expected, the effect of the reception of nuclei by the MSU of recrystallized grains contributes as a grain refinement since equation (I-65) gives a negative term. When the structure is entirely recrystallized, the MSU of recrystallized grain is the only one that contains grains and it interacts only with itself. The sweeping of its boundaries produces a grain size increase through equation (I-54). And nucleation (its own actually) tends to reduce its grain size with equation (I-65). As a consequence, the geometric framework provides in itself a tendency for the model to reach a dynamic steady state.

From that point, all geometry aspects are set and the geometric framework is locked. It needs two types of input:

- nucleation rates and nuclei size,
- the terms of grain boundary velocities $\dot{u}_{ij}$, to make the grains grow or be consumed through grain interactions.

Now, the second part will discuss how these nucleation and migration rates are calculated along with other driving forces and mechanisms.

II. Driving forces and mechanisms

Driving forces can be parted into three main groups which fit the usual sequence of discontinuous dynamic recrystallization: “energy storage – nucleation – growth”. So the first driving forces deal with dislocation generation and recovery, the second with sub-boundary generation and disorientation, which lead to nucleation, and the last with boundary migration. To begin, equations used to represent these driving forces will be presented, for each of the three groups. Then, the actual order in which they are used, in relation with the geometric framework will be discussed.

II.A. Equations representing driving forces

II.A.1. Equations related to dislocation behavior

As plastic deformation occurs, the first activated mechanism is the generation of dislocations. It is coupled with dynamic recovery to control the increase of stored energy. To represent them, various formulations have been proposed in literature. The most common one was proposed by Laasraoui and Jonas [8]. Their formulation assumes a constant mean free path of dislocations, and a recovery rate that is proportional to dislocation density. It leads to an initial rounded shape of stress strain curves, which fits well austenitic steel behavior for instance. But it does not fit the one observed on nickel base superalloys, which tend to exhibit a linear increase of the stress at low deformations (Figure II-1).

Expressions that connect the mean free path of mobile dislocations with the average distance between forest dislocations provide a linear increase of the stress. Such a formulation was applied to Superalloy 718 [9]. It was chosen for this model too, though presented differently. Starting with the Orowan equation (II-1), it is possible to deduce a form for which parameters have a more apparent physical meaning.

$$\dot{\varepsilon} = \beta b \dot{\rho}^{+} L = \beta b \dot{\rho}^{+} n \sqrt{\frac{3}{\rho}} \approx \frac{nb}{\sqrt{\rho}} \dot{\rho}^{+} \qquad \text{(II-1)}$$

In this equation, β is a geometric coefficient between 0.5 and 1, b is Burgers' vector and L is the mean free path of newly generated dislocations. The latter is supposed to be proportional to the average distance between the already existing dislocations. So n is the average number of forest dislocations crossed by mobile dislocations before they are definitely stopped. The last form of equation (II-1) results from considering that the actual value of β is about the inverse of the square root of 3, i.e. 0.57. Finally one gets the expression of dislocation generation in equation (II-2).

$$\dot{\rho}^{+} = \dot{\varepsilon} \frac{\sqrt{\rho}}{nb} \qquad \text{(II-2)}$$

Dynamic recovery is supposed to verify equation (II-3), and so is it for metadynamic recovery too, but with other values for the coefficients r and a.

$$\dot{\rho}^{-} = r \rho^{a} \qquad \text{(II-3)}$$

Both n and r are supposed to be the multiplication of a power law of the strain rate by an Arrhenius law to account for temperature dependence.

It is possible to identify the value of power a in the case of dynamic recovery from stress-strain curves. Equation (II-4) is commonly used to link flow stress and dislocation density. It has been widely verified for pure metals, but using it for superalloys at high temperature may rely on a rather strong assumption. Nevertheless, one can use it as a first order approximation.

$$\sigma = \sigma_0 + \alpha G b \sqrt{\rho} \qquad \text{(II-4)}$$

σ_0 is supposed to be a constant for a given curve, α is about 0.5, and G is the shear modulus. Equation (II-5) comes by derivation and inversion of (II-4).

$$\frac{d\rho}{d\varepsilon} = \frac{2\sqrt{\rho}}{\alpha G b}\frac{d\sigma}{d\varepsilon} \tag{II-5}$$

Then one can write the apparent recovery rate with equation (II-6).

$$\frac{d\rho^{-}}{d\varepsilon} = \frac{d\rho^{+}}{d\varepsilon} - \frac{d\rho}{d\varepsilon} = \frac{\sqrt{\rho}}{b}\left(\frac{1}{n} - \frac{2}{\alpha G}\frac{d\sigma}{d\varepsilon}\right) \tag{II-6}$$

And finally, by combining equations (II-6) and an inversion of (II-4), equation (II-7) comes as an expression of the apparent recovery rate.

$$\frac{d\rho^{-}}{d\varepsilon} = \frac{\sigma - \sigma_0}{\alpha G b^2}\left(\frac{1}{n} - \frac{2}{\alpha G}\frac{d\sigma}{d\varepsilon}\right) \tag{II-7}$$

In the case of Waspaloy, the application of equation (II-7) to the curves of figure (II-1) obtained at $0.1s^{-1}$ reveals that the apparent dynamic recovery rate depends linearly on the dislocation density, as shown in Figure (II-2). Thus in the case of dynamic recovery of Waspaloy, the value of coefficient a is 1. The increase of the apparent recovery rate over the linear law is a signature of dynamic recrystallization, which provides an additional softening term. The fact that the apparent recovery rate becomes negative or that the dislocation density can come back to 0 illustrates that the actual equation for the stress is more complex than (II-4). The latter can only be used as a local approximation to give an idea of the dislocation density variation, for instance at the beginning of the stress-strain curve.

II.A.2. Equations related to sub-boundaries and nucleation

A previous investigation revealed that nucleation in Superalloy 718 comes from the local disorientation of some sub-grains [4]. A model connecting sub-boundary generation and disorientation to nucleation was designed. In the case of Waspaloy, the existence of nucleation on second phase particles shows that the same kind of mechanism is active. As a consequence, in this model too, nucleation was connected to

sub-boundary evolution. However, the disorientation process was simplified a lot in order to get some margins in terms of managed complexity for other aspects. To deal with the case of Waspaloy, or more generally of coarse ingot grains, two kinds of sub-boundary/nucleation have to be modeled (necklace and volume). In addition, the observed dependence of recrystallization rate with crystallographic orientation [5] could be expected to come mostly from sub-boundary evolutions [10].

Few variables have to be added to the microstructure description to represent aspects related to sub-boundaries. For every MSU i, two sub-boundary densities $S_{sb\,i}$ and $S_{sbv\,i}$, and two disorientation parameters x_i and $x_{v\,i}$ are defined, respectively for necklace and volume sub-boundary/nucleation. The Taylor factor of the MSU is noted $M_{T\,i}$. In the next equations, the index i will not be mentioned as equations of sub-boundary evolution do not depend on the MSU number.

Six equations are needed to allow the representation of sub-structure evolutions and of nucleation. They are grouped by three. Each group is formed of an equation for sub-boundary generation, one for sub-boundary disorientation, and one for the conversion of sub-boundaries into new mobile boundaries. The latter will be converted into a nucleation rate. The first group leads to necklace nucleation, and the second one to volume nucleation. However, when grains are not coarse enough, bubbles topology is not allowed by the geometric framework. In such a case, the few so-called volume nuclei that are generated are simply added to the necklace ones.

The expressions chosen for “necklace” and “volume” sub-boundary generations are presented in equations (II-8) and (II-9) respectively.

$$\dot{S}_{sb}^{+} = k_G \exp\left(\frac{Q_G}{RT}\right)\dot{\varepsilon}\,F\left(M_T\right)\exp\left(-\frac{D}{D_G}\right) \qquad \text{(II-8)}$$

$$\dot{S}_{sbV}^{+} = k_{GV} \exp\left(\frac{Q_{GV}}{RT}\right)\dot{\varepsilon}\,F_V\left(M_T\right) \qquad \text{(II-9)}$$

k_G, k_{GV}, Q_G, Q_{GV} and D_G are coefficients to identify. R is the universal gas constant. F and F_V are functions of the Taylor factor. Since tests on ingot microstructures have been performed for three Taylor factor, three values were actually identified for F and F_V. Interpolation of these values has not been investigated yet.

Disorientation variables are abstract ones. x and x_V are to be seen as indicators of levels of disorientation of the sub-structure. Nucleation starts when they reach the unit. But nothing prevents them from increasing above the unit. In practice, it would be difficult to manipulate parameters representing these abstract disorientation rates. So the model uses equations of critical strain. They are simply the inverse of the disorientation rate since the critical value for x and x_V is the unit. Equations for critical strains are the same for both "necklace" and "volume" sub-boundaries, just with different values for their parameters. The equation used is (II-10).

$$\varepsilon_c = k_c \exp\left(\frac{Q}{RT}\right) F_c\left(M_T\right) \tag{II-10}$$

k_c and Q_c are coefficients to identify. For the volume, though the equation is not written, equivalent coefficients are $k_{c\,V}$ and $Q_{c\,V}$. F_c and $F_{c\,V}$ are functions of the Taylor factor, for which three values have actually been identified for both. Disorientation rate is deduced easily from previous explanations as shown in equation (II-11).

$$\dot{x}^+ = \frac{\dot{\varepsilon}}{\varepsilon_c} \tag{II-11}$$

Conversion of sub-boundaries into mobile boundaries is managed by equations (II-12) and (II-13), when x and x_V are greater than 1.

$$\dot{S}_{sb}^{\ -} = \dot{S}_b^+ = k_N\, \dot{\varepsilon}\left(x-1\right) S_{sb} \tag{II-12}$$

$$\dot{S}_{sbV}^{\ -} = \dot{S}_{bV}^+ = \left(k_{NV} + k_{NB} S_B^{\,p}\right) \dot{\varepsilon}\, \left(x-1\right) S_{sbV} \tag{II-13}$$

K_N, k_{NV}, k_{NB} and p are coefficients of the material. S_B is the surface of bubbles per volume unit in the considered MSU, calculated by the geometric framework, thanks to equation (I-19). The conversion of some sub-boundaries into grain boundaries leads to an apparent decrease of the disorientation of remaining sub-boundaries, as shown in equation (II-14). Equivalent equation is used for "volume" sub-boundaries.

$$\dot{x}^{-} = x\frac{\dot{S}_{sb}^{-}}{S_{sb}} \tag{II-14}$$

Nuclei size D_N is given by equation (II-15) in which, once again, k_D and Q_D are coefficients of the model.

$$D_N = k_D \exp\left(-\frac{Q_D}{RT}\right) \tag{II-15}$$

A division of generated boundary surfaces by the surface πD_N^2 of a nucleus gives the nucleation rates, which are the first input of the geometric framework. Its second input, boundary velocities, is going to be presented in the following paragraph.

II.A.3. Grain boundary migration

The classic equation of Turnbull (II-16) connects the driving force P seen by a boundary with the boundary velocity $\dot{u}$, through the definition of M as the grain boundary mobility.

$$\dot{u} = MP \tag{II-16}$$

Boundary mobility depends on temperature and is subjected to solute drag effects and disorientation dependence. Since it represents the average mobility of the grain boundaries of the microstructure, and integrates a lot of different cases, it is not possible to write it based on analytic expressions. The expression used for the average grain boundary mobility of a set of grains is equation (II-17). P_0 is defined as the grain boundary tension of a 1µm grain, as shown in (II-18). γ is the grain boundary energy. λ

is a coefficient to identify. M_0 is written as an Arrhenius law whose activation energy is noted Q_M, and pre-exponential coefficient is called K_M.

$$M = M_0 \left(\frac{P}{P_0} \right)^{\lambda} \tag{II-17}$$

$$P_0 = \frac{\gamma}{2 \times 1 \mu m} \tag{II-18}$$

Two types of driving forces are accounted for: energy stored as dislocations and sub-boundaries P_D, and grain boundary energy P_S. The latter is shown in equation (II-19).

$$P_S = \frac{\gamma}{2D} \tag{II-19}$$

Factor 1/2D, instead of 1/R+1/R=4/D comes from the fact that the actual curvature of grain boundaries is lower than the inverse of the grain radius.

The dislocation density ρ_{sb} stored into sub-boundaries is related to their disorientation θ through equation (II-20). N is the number of dislocation families present into the sub-boundary. Typically, to represent any kind of crystallographic rotation between two sub-grains, N has to be at least equal to 3. As disorientation is not really calculated in the model, it is necessary to rely on an average value of θ. As superalloys are low stacking fault energy alloys, θ cannot be very high. A value of 3° i.e. approximately 0.05 radians is reasonable.

$$\rho_{sb} = \left(S_{sb} + S_{sbV} \right) \frac{N\theta}{b} \tag{II-20}$$

When it comes to evaluate their energy contribution, sub-boundary dislocations are to be accounted for with about an order of magnitude lower than free dislocations, as shown in equation (II-21) is 0.1.

$$P_D = \frac{Gb^2}{2}\left(\rho + 0.1\rho_{sb}\right) \quad \text{(II-21)}$$

Evaluation of the difference of energy seen by a boundary depends on the type of grain interaction. For interaction between grains of the same MSU, the difference of dislocation density is expected to be low. It will be considered as one tenth of the actual average dislocation density of the grains. The energy of grain boundaries will be accounted for at its full potential. The driving force seen by a grain boundary between grains of the same MSU i is written in equation (II-22).

$$P_{i-i} = 0.1P_{Di} + P_{Si} - P_Z \quad \text{(II-22)}$$

P_Z is the Zener pining force due to precipitates. It slows down grain boundary migration or can even block it. It is null when there are no precipitates in the microstructure, i.e. typically when deformation is performed above the solvus temperature of δ or γ', depending on the considered superalloy. Expressions of this coefficient have not been identified yet for Waspaloy. However, they should be similar to those used in a previous model of microstructural evolution of Superalloy 718 [4].

For interactions between grains of different MSUs, equation (II-23) only accounts for the difference of energy that comes from different dislocation densities on the two sides of the grain boundary. Taking into account the grain boundary tension as a term opposed to the grain growth was tested. It brought out very instable behavior and difficulties to fit the model using simple equations and coefficients. This comes from the fact that when nuclei have just appeared, their size is low and thus their boundary tension is very high. But this is compensated by a higher local dislocation density due to the nature of nucleation sites. This higher local energy allows nuclei growth. As nuclei diameter reaches few microns more than their initial size, grain boundary tension decreases a lot. Simultaneously, boundary gets out of high energy areas, a bit distant from nucleation sites, where dislocation density is more homogeneous and close to the

average one of grains. Taking properly into account the grain boundary tension for interactions between grains of different MSUs would require calculating one or several additional terms with little or even no benefit. As a consequence, the model neglects these very local aspects, as other models usually do [3, 9].

$$P_{i-j} = P_{D\,j} - P_{D\,i} \pm P_Z \tag{II-23}$$

These equations allow the evaluation of the various driving forces represented in the model. But the order in which these evaluations are actually performed is different from the natural one that has just been used.

II.B. Actual order of evaluation of driving forces and mechanisms

The algorithm of integration of the model relies on a first order scheme. The high number of variables and relationships between them, especially in the geometric framework, has prevented us until now from developing a second order scheme of integration that satisfies conservation laws. Each increment is calculated in two steps. The first is an evaluation of the derivatives of all variables. Only then, integration itself is carried out.

The order in which the rates of variation of variables are calculated is actually almost the opposite of the one that could be expected, mostly due to calculation speed considerations. The first operations consist in a loop that performs two kinds of evaluations for each MSU successively:

- the evaluation of the driving forces P_{Di} and P_{Si} of the grains of each MSU i., using equations (II-19) and (II-21).
- the calculation of boundary and bubbles surfaces is carried out using the laws of the geometric framework expressed by equations (I-12), (I-14), (I-19) and (I-49). As the loop is incremented, total boundary surfaces are progressively calculated to match equations (I-20), (I-21) and (I-22).

Then, a new loop over all MSUs of the microstructure is performed to calculate the probability parameters resulting from equations (I-23) to (I-28). At the end of this loop, the framework is ready for the evaluation of interaction probabilities, and then to receive its first input: the grain boundary velocities for each pair of MSUs. Two intricate loops are defined so that every pair i-j is calculated only once, knowing that interaction j-i is the complementary of i-j. Calculating i-j and j-i together constitutes a faster algorithm and provides an additional security to insure volume conservation. So, at each increment of these loops, interactions i-j and j-i are calculated with:

- the velocity rates $\dot{u}_{ij}$ that come from equations (II-22), (II-23) and (II-17).

- the rates of variation of the volume of grains, of the dimensions of grains and of the volume of MSUs. They are stored in temporary variables. For each MSU, volume variations of grains are actually summed into two intermediate variables. One stores the sum of positive contributions to volume variation, and the other stores the sum of negative ones. Depending on the type of grain interaction, the equations to use are (I-29) to (I-31), or (I-32) to (I-37), or (I-40) to (I-42) and (I-45), or (I-52) to (I-54) and (I-57). The latter is actually (I-45) again.

Following calculations are only performed if the strain rate is strictly positive.

Through a new loop, for each MSU, the calculation of sub-boundary generation is performed using equations (II-8) and (II-9). Evaluations of nucleation rates follow with equations (II-12) and (II-13), combined with equation (II-15). Nucleation rates are stored into temporary variables. These calculations provide the necessary data to use equations (II-10), (II-11) and (II-14) that manage disorientation rates.

Once sub-boundary evolution and nucleation for all MSUs have been calculated, stored nucleation rates provide the second input of the geometric framework to evaluate additional variations of volume and size of grains through equations (I-58) to (I-62) and (I-63) to (I-66).

Then, for each MSU, the rate of variation of dislocation densities is calculated thanks to equations (II-2) and (II-3). If the strain rate is null, only the metadynamic version of equation (II-3) has to be applied.

To finish, for any strain rate, the effects of grain volume variations on dislocation densities and sub-boundary densities have to be taken into account. They depend on the sign of the volume variation, which explains why contributions to volume variations were stored into two different intermediate variables for each MSU. Firstly, positive volume variations of grains induce a softening term through a decrease of these densities. This softening term results from the multiplication of the considered density by the ratio of the positive volume variation of the grain over its volume. It can be understood as a dilution of the considered density into a larger volume. Secondly, a parameter K_{absorb} is defined to represent the heterogeneity of repartition of sub-boundaries in grains. As nucleation comes from sub-boundaries, it tends to happen in areas where sub-boundary densities are greater than their average value. Then, when nuclei grow, they tend to consume these areas first, which induces an apparent decrease of the average sub-boundary density of the grain that is consumed. This apparent decrease is treated as an additional softening term of sub-boundary densities. It is calculated as the product of K_{absorb} by the ratio of the negative volume variation of the grain over its volume. This last term is extremely important to represent the progressive decrease of the recrystallization rate during metadynamic recrystallization.

After the evaluation of the rate of variation of all the variables of the structure, integration at the first order comes naturally from adding to each variable the product of its total variation rate by the time increment. However, as long as volume nucleation has not started, and for grains that are not supposed to support bubbles topology, a numerical security is applied. It consists in deducing the volume of the grain not from its integration but directly from the new grain dimensions. It insures that the volume of the grain and the one of the envelope are strictly identical, and that no bubble will

appear due to the accumulation of some numerical error. To finish, for each MSU, grain density is updated as the ratio of the volume of the MSU over the unit volume of the grains it contains. Then the microstructure is ready for a new increment.

II.C. Measurement simulation

In order to solve the model, it is necessary to extract from the microstructure the various values that have to be compared with the measured ones: a measurement simulation has to be performed.

Recrystallized fraction is simply the volume of the MSU of highest index, N_{MSU-1},, as it receives the nuclei produced by the microstructure. Recrystallized grain size is deduced from the size of the grains of this MSU too. In order to represent the effect of a section, which tends to give a lower value than the volume diameter, the grain size of the MSU is multiplied by the square root of 2/3. This value comes from stereological considerations that will not be detailed here. If several hits have been calculated and some recrystallized grains of previous hits are stored in MSUs of lower index, the total recrystallized fraction is the sum of the volumes of these MSUs. And the average grain size (if it makes sense) is supposed to be the average of the grain size of each MSU, balanced by its volume.

In the case of wrought initial microstructures, the size of the remnants of initial grains is calculated with the same method as for recrystallized ones. However, for ingot microstructures, the size of remnants of initial grains cannot be evaluated in the same way. In this case, the apparent size of remnants is considered to be the size of the cells that are delimited by the percolated bubbles of recrystallized grains. At low values of bubbles fraction, such assertion makes almost no sense. But when the fraction of bubbles reaches about 50%, most of the bubbles are in contact with others. They define a volume network that isolates unrecrystallized areas from each other, even if they originate from the same initial grain. If these cells are supposed to be based on the

shape of a dodecahedron, delimited such that each face contains a particle involved in volume nucleation, one can conclude that the volume of a base-cell is the one containing six of these particles. Then, assuming that a base-cell is similar to a sphere, its size is supposed to be given by equation (II-24). And the size of remnants of initial grains in a section is estimated by equation (II-25).

$$D_{cell} = \left(\frac{36}{\pi n_{PSN}} \right)^{1/3} \tag{II-24}$$

$$D_{remnants} = \sqrt{\frac{2}{3}} D_{cell} \left(1 - X_b\right)^{1/3} \tag{II-25}$$

III. Application to Waspaloy

The model architecture that has been described until now was design so that it is applicable to various alloys. However, equations were chosen to fit the behavior of Waspaloy. Thus, for other superalloys, some modifications of equations may be necessary in order to take into account other dependencies that have been neglected, or suppress some of them, as they may not be required. However, even if this part will deal with the resolution of the model specifically for Waspaloy, its topic is to propose a method of resolution and identification of coefficients that should be applicable to other alloys too.

As one could see in the two first parts, the meso-scale mechanism-based model is very different from one based on the Avrami equation. One can expect that the resolution method is very different too. It is not possible to identify all parameters at the same time as it is done with a model based on the Avrami equation, using multi-linear regression methods. In the Avrami-based model, coefficients have little physical meaning, so almost any value that fits experimental data is acceptable. On the contrary, the model that was designed here relies on coefficients that aim at representing driving forces and their dependencies with microstructure or thermomechanical values, even when equations may look very simplified and far from reality. In addition, it cannot be solved using analytical techniques as multi-linear regressions. Only numerical optimization can be used. Therefore, an initial solution has to be identified, at least on some specific areas of the model. The first of these areas, which anybody may think *a priori* as the last to solve, is static grain growth.

III.A. Identification of parameters of static grain growth

Static grain growth is the simplest regime that the model has to manage. It only involves grain boundary tensions and grain boundary mobility. Grain boundary energy

is usually approximately known, a least its order of magnitude. For nickel and its alloys, it is about 0.7-0.9 Jm^{-2} [11, 12]. For this model, it was considered to be 0.7 Jm^{-2}.

When the model is reduced to the static grain growth of one single MSU, it is possible to obtain analytical solutions, depending on the value of parameter λ in equation (II-17). Firstly, the driving force is given by equation (III-1). The grain boundary velocity is then written in equation (III-2).

$$P = \frac{\gamma}{2D} \tag{III-1}$$

$$\dot{u} = M(P)\,P = M_0 \left(\frac{1\mu m}{D}\right)^{\lambda} \frac{\gamma}{2D} \tag{III-2}$$

The volume swept by boundaries ($S_b \dot{u}$) induces a decrease of the boundary density ($S_b = \frac{3}{D}$), which means that $\dot{S}_b^{-} = S_b^2 \dot{u} = \frac{9\dot{u}}{D^2}$. Finally, the grain size has to verify differential equation (III-3), of which solutions are of the form of equation (III-4).

$$\dot{D} = \frac{3M_0\gamma}{2D}\left(\frac{1\mu m}{D}\right)^{\lambda} \tag{III-3}$$

$$D^{\lambda+2} - D_0^{\lambda+2} = kt \tag{III-4}$$

Previous investigation [2] provides equation (III-5) for static grain growth in which the exponent on D is 3 (D in meters). As a consequence, coefficient λ has to be equal to 1: average grain boundary mobility of a microstructure is approximately proportional to its average driving force. In the specific case of λ=1, equation (III-4) becomes equation (III-6) with D in meters.

$$D^3 - D_0^3 = 2 * 10^8 \exp\left(-\frac{595000}{RT}\right) t \tag{III-5}$$

$$D^3 - D_0^3 = 4.5 * 10^{-6} * M_0 \, \gamma \, t \qquad \text{(III-6)}$$

Identification of parameters leads to a first estimation of M_0 in equation (III-7), in $m^4 J^{-1} s^{-1}$.

$$M_0 = 6.35 * 10^{13} \exp\left(-\frac{595000}{RT} \right) \qquad \text{(III-7)}$$

Once grain boundary mobility can be evaluated, it is necessary to get the order of magnitude of dislocation densities to generate through deformation such that recrystallization rates are reproduced by using this mobility.

III.B. Order of magnitude of dislocation densities

It is difficult to evaluate grain boundary migration rates during deformation from measurements of recrystallized fractions because nucleation contributes to the overall recrystallization rate too. On the contrary, the metadynamic regime provides an interesting insight because only the migration of grain boundaries that are the interface between recrystallized and initial grains is responsible for the recrystallization fraction increase. If one can estimate the migration rate of these grain boundaries during metadynamic evolution, then, provided an estimation of the grain boundary mobility, he can deduce at least the order of magnitude of dislocation density.

To do that, a model of recrystallization based on the Avrami equation was designed on data provided by Shen [2], though in a special form for the metadynamic regime. Obtained expressions are presented in equations (III-8) to (III-11).

$$\varepsilon_{0.5} = 4.6 * 10^{-5} \exp\left(\frac{110000}{RT} \right) \dot{\varepsilon}^{0.078} \qquad \text{(III-8)}$$

$$X_{dyn} = 1 - \exp\left(-\ln(2) \left(\frac{\varepsilon - 0.17}{\varepsilon_{0.5}} \right)^{4.2} \right) \qquad \text{(III-9)}$$

$$t_{0.5} = 8*10^{-7} \exp\left(\frac{160000}{RT}\right) \varepsilon^{0.388}\, \dot{\varepsilon}^{0.06}\, D_0^{0.387} \qquad \text{(III-10)}$$

$$X_{m-dyn} = X_{dyn} + \left(1 - X_{dyn}\right)\left[1 - \exp\left(-\ln(2)\left(\frac{t}{t_{0.5}}\right)\right)\right] \qquad \text{(III-11)}$$

The latter insures that the model is continuous from the dynamic to the metadynamic regime. If one assumes that the size of the remnants of initial grains follows equation (III-12) during the metadynamic regime, then the disappearance rate of these grains is connected to the recrystallization rate. It leads to the estimation of the grain boundary velocity of interfaces between initial and recrystallized grains, as written in equation (III-13). And finally, the apparent dislocation density that corresponds to such a grain boundary velocity is given by equation (III-14) when λ=1.

$$D_{remnants} = D_0 \left(1 - X_{m-dyn}\right)^{1/3} \qquad \text{(III-12)}$$

$$\dot{u} = \frac{2D_0}{3} \frac{\dot{X}_{m-dyn}}{\left(1 - X_{m-dyn}\right)^{2/3}} \qquad \text{(III-13)}$$

$$\rho = \frac{2}{Gb^2}\sqrt{\frac{\dot{u}\, P_0}{M_0}} \qquad \text{(III-14)}$$

The latter was calculated for each metadynamic recrystallized fraction published in Shen's article. No clear dependence could be identified with strain, strain rate or initial grain size. Only the temperature and holding time have clear influence on the evolution of the apparent dislocation density, as one can observe on Figure (III-1).

At 1177°C (2150F), extrapolated values of dislocation densities at the end of deformation would match approximately the amplitude of variation of dislocation densities found on Figure (II-2), which was drawn at the occasion of a discussion about strain hardening and dynamic recovery. If it appears on that figure that, though

maximum dislocation density is roughly the same, both n and r change a lot from the first hit to the second, while temperature and strain rate are the same. The only noticeable change between the two hits conditions is the initial grain size. Since the amplitude of variation of apparent dislocation density is roughly the same for both hits, instead of trying to identify n and r, it is easier to manipulate n and the product nr. It is related to the dislocation density given by the equilibrium of strain hardening (equation II-2) and dynamic recovery (equation II-3) given by equation (III-15). Manipulating n and ρ_{eq} insures that changing n will only affect the strain hardening rate, without changing the maximum level of stored energy that will be reached, as r is adjusted to compensate the variation of n.

$$\sqrt{\rho_{eq}} = \frac{\dot{\varepsilon}}{bnr} \qquad \text{(III-15)}$$

Then, one can obtain orders of magnitude of these parameters. The number of forest dislocations crossed by mobile ones before they are stopped, n, could be set to vary between 10 and 30, as a first guess, given the amplitude of temperature on which the model has to function. A variation of the equilibrium dislocation density, at $1s^{-1}$, between 150 at 1000°C and 20 at 1120°C looks reasonable. Then a first estimation of values of r is deduced: about 30 at 1000°C and 45 at 1121°C. Sensibilities of n and r to the strain rate are supposed to be negligible as a first guess, because strain rate could not be identified as a strong discriminator in Figure III-1, contrarily to time and temperature.

From that point, the model is known to have reasonable initial values of grain boundary mobility, strain hardening and dynamic recovery. Values of critical strain can be initialized to about 0.1. Influence of the Taylor factor is neglected in the initial solution. The size of nuclei can be set to vary between 5 and 10 microns. There is no clear method to guess initial values of sub-boundary generation. But since all other values can be initialized understandably, remaining ones can be adjusted manually in order to

obtain the first solution, and then start the process of calibration and numerical optimization of all parameters simultaneously. To manage these adjustments, specific software dedicated to the treatment and resolution of such recrystallization models was designed.

III.C. Recrystallization modeling software: RX-MOD

The first version of this software was designed to develop a model of microstructural evolution of wrought Superalloy 718 [4]. It was modified and extended to manage all the data and calculation management tasks required to develop models dealing not only with wrought but also ingot microstructures. Emphasis has to be put on the fact that it would be highly hazardous to try to develop mechanism-based models that aim at being optimized, especially for industrial application, without having such toolbox available. The RX-MOD software architecture is organized around seven modules, each of them being a specific set of tools.

The first one is the experimental database. It contains the nominal definition of each test that was performed. For each characterized microstructure, a set of values of grain sizes, recrystallized fractions… etc. is to be completed with measured data. Each value is doubled in order to store the results given by the model and allow later comparison of measured and calculated values.

A thermomechanical module aims at estimating the actual evolution of temperature in samples, using finite difference methods of integration inspired from those proposed in literature [13]. Among other aspects, it calculates the heating due to deformation and cooling rates during quenching. The overall role of this module is to allow taking into account, for every test defined in the experimental database, the difference between its nominal definition and the actual path of solicitation seen by the point where the microstructure was characterized. When the calculation would be too complex for this

rather simple module, it is possible to initialize the thermomechanical path using data provided by an FEM tracking point.

The core of the software is the module that performs the integration of the model on the thermomechanical path. It controls the stability of integration in order to optimize the time step at each increment. This control is performed by the executable of the software, but the model itself, all what has been presented in parts I and II of this paper, is externalized into a dynamic linked library (DLL). As a consequence, just changing the name of the DLL to load allows running another model of recrystallization.

A module, part of the DLL, carries out measurement simulations. From a microstructure made of MSUs, it extracts the values that are to be stored in the experimental database, taking into account section effects for instance.

To perform numerical optimization, a module using gradients algorithms (Fletcher-Reeves and Ribière-Polak) can modify the parameters of the model in order to reduce an average error defined in the experimental database. This module still needs improvements to accelerate the stability and convergence of its algorithms.

A module that loads data extracted from Deform® calculations can perform the integration of the model on each node of a bi-dimensional (2D) FEM mesh. Calculations on 3D-meshes have not been tested yet and will need adjustments. They are the ultimate goal of the current study, since the model is designed for the primary processing of ingots, especially cogging.

Finally, a graphic editor gives access to the comparison of measured and calculated data, in order to identify model weaknesses, during the calibration process. It also draws maps of the various values provided by the model when applied to FEM calculations.

III.D. Microstructure initializations

Microstructures are initialized as a set of five MSUs. The two first MSUs (indexes 0 and 1) are for initial grains. They support bubbles topology if initial grains are coarse enough, i.e. for ingot microstructures. In such a case, they support grain anisotropy too in order to account for the columnar shape of grains, with an anisotropy ratio of 10 (D_z/D_x=10, and D_x=D_y=5000µm [5]). The volume partition between the two MSUs is 90%-10%. The Taylor factor of <100> grains in uniaxial compression, which is 2.45, is affected to the second MSU in order to represent grains that tend to have a low recrystallization rate and may remain as ALAs. The first MSU is given the main Taylor factor of the microstructure. For wrought initial microstructures, it is 3.06, i.e. the average Taylor factor of f.c.c. random texture in uniaxial compression. For ingot microstructures, if the main axis of columnar grains is transverse to the compression axis, it will be 3.1, if the axis is at 45°, it will be 3.55, and if they are parallel, it will be 2.45. The same grain size is given to these two MSUs: it is the initial grain size measured, multiplied by the square root of 3/2, so that when the measurement section is simulated as described in II.C, it results in the expected initial grain size.

The MSU of highest index, 4, contains recrystallized grains. It is initially void. It receives the nuclei generated during the current deformation as defined in the geometric framework. If another deformation is performed, then, just before it starts, recrystallized grains of MSU 4 are transferred into the two intermediate MSUs (indexes 2 and 3), where the recrystallized grains that appeared during previous hits are stored. 90% of recrystallized grains go to MSU 2, and 10% go to MSU 3, and their Taylor factors are supposed to be respectively 3.06 and 2.45. This is necessary in order to be consistent with the initialization method applied for MSUs 0 and 1: after several hits, when MSUs 0 and 1 have completely disappeared, if a new hit is performed, MSUs 2 and 3 are going to behave as a wrought microstructure that would have been initialized in MSUs 0 and 1, and the model will behave the same way.

III.E. Parameters identification

To carry out the resolution, all available data from Shen [2] and Weaver [5] were filled in the database. The first goal was to reach an average error on recrystallized fractions lower than 10% before thinking about tests on industrial applications and identification of model weaknesses. It is actually 9.5%. Three “error graphs” that represent calculated recrystallized fractions vs. measured ones are presented in Figures (III-3). Recrystallized fractions measured after long holding times on ingot microstructures exhibit the highest discrepancy, especially when grains axis were at 45° from the compression axis. It comes from the fact that 45° microstructures have the widest range of Taylor factors: the actual energy stored in grains at the end of deformation may be far from the average one calculated using the model. Then, integrated on several minutes or hours, such differences induce a larger discrepancy of recrystallized fractions. Given the size of initial grains, very few were covered by characterized areas. It explains why the model exhibits poor precision on this set of data. If these are not included, the average error is down to 8.4%, and even 7.3% if all ingot metadynamic recrystallized fractions are excluded.

The parameters of driving force equations that were used to obtain these results are going to be presented. But first, the only parameter of the geometric framework is given: the best value for the density (n_{PSN}) of particles on which volume nucleation can happen, was found to be 20 particles per cube millimeter. It gives an inter-particular distance of about 450µm. It is in agreement with the typical distance between bubbles observed on micrographs [5].

To manage equation parameters in an easier way, the software requires the definition of two reference temperatures that are used to avoid manipulating Arrhenius equation parameters directly. These two temperatures have been set to 1000°C (1832F) and 1177°C (2150F). So, for all parameters that depend on temperature, their values will be

given at these two reference temperatures, along with corresponding Arrhenius coefficients (pre-exponential and apparent activation energy).

III.E.1. Grain boundary mobility

The actual apparent activation energy of grain boundary mobility is slightly greater than the first guess coming from Shen's article, as one can see on equation (III-16), in $\mu m^3 N^{-1} s^{-1}$.

$$M_0 = 9.4 * 10^{32} \exp\left(-\frac{618291}{RT}\right) \quad \text{(III-16)}$$

At 1000°C, M_0 = 4.0 10^7 $\mu m^3 N^{-1} s^{-1}$ = 4.0 10^{-11} $m^3 N^{-1} s^{-1}$.

At 1177°C, M_0 = 5.0 10^{10} $\mu m^3 N^{-1} s^{-1}$ = 5.0 10^{-8} $m^3 N^{-1} s^{-1}$. This value may seem overestimated. But one has to remember that it is the mobility for the grain growth of a 1µm grain, which never happens at so high temperatures. Maybe, a saturation value of the grain boundary mobility should be implemented, though it has not been necessary to solve the model (Figure III-5). Driving forces provided by the model, at a given temperature, may always stay lower than the one required to reach such a saturation value.

III.E.2. Dislocations related equations

The average number of dislocations crossed by the newly generated ones before they are stopped is given by equation (III-17).

$$n = 9.0 * 10^5 \exp\left(-\frac{111064}{RT}\right) \dot{\varepsilon}^{-0.08} \quad \text{(III-17)}$$

At 1s^{-1} and 1000°C, n = 2.5, and at 1177°C, n = 9. These values are quite lower than the ones initially estimated, by about a factor 5. These are necessary to fit the observed metadynamic recrystallization rates for low deformations (about 0.2), which are almost as high as those obtained for greater strains. It is possible that near the first sites of

nucleation, dislocation density increases a lot faster than the macroscopic one which defines the stress evolution.

Equilibrium dislocation density is given by equation (III-18).

$$\rho_{eq} = 1.3 * 10^{-6} \exp\left(\frac{200000}{RT}\right) \dot{\varepsilon}^{0.08} \qquad \text{(III-18)}$$

At $1s^{-1}$ and 1000°C, ρ_{eq} = 200 μm^{-2} = 2 10^{14} m^{-2},

and at 1177°C, ρ_{eq} = 20 μm^{-2} = 2 10^{13} m^{-2}.

Equilibrium dislocation density exhibits a low dependence with temperature. It is even more interesting to notice it because, on the contrary, grain boundary mobility is extremely dependent with temperature. One could think it is overestimated. If it were, equilibrium dislocation density would have a very high temperature dependence in order to compensate it and provide, through the product of mobility and stored energy, the appropriate recrystallization rates. The low temperature dependence of equilibrium dislocation density proves that the dependence of grain boundary mobility with temperature, though very high, probably due to solute drag effects, is actually a required minimum.

The values of dynamic recovery rate are obtained from equation (III-15).

At $1s^{-1}$ and 1000°C, r =113, and at 1177°C, r = 100. Since values of n, which include local behavior, are under evaluated, those of r are over evaluated in order to compensate and reach the necessary equilibrium dislocation density anyway. It can be expected that their macroscopic counterpart should be about 5 times lower.

Metadynamic recovery rate is given by equation (III-19).

$$r_{m-dyn} = 3.1 * 10^{9} \exp\left(-\frac{314250}{RT}\right) \qquad \text{(III-19)}$$

At 1000°C, $r_{m\text{-}dyn}$ = 4 10^{-4} $\mu m^2 s^{-1}$ and at 1177°C, $r_{m\text{-}dyn}$ = 1.5 10^{-2} $\mu m^2 s^{-1}$. The value of power a, which was equal to 1 for dynamic recovery, is difficult to adjust for metadynamic recovery. Three values, 1.0, 1.5 and 2.0, were tested. It is possible to adjust the overall behavior by adjusting $r_{m\text{-}dyn}$ in consequence. However, to fit the metadynamic recovery of wrought microstructures, a value of 2 was the best, while 1 or 1.5 suited better the metadynamic evolution of ingot microstructures. The value of $r_{m\text{-}dyn}$ given here is for a=2. Such metadynamic recovery rates are able to bring dislocations densities to almost zero in times of 10 seconds to 2-3 minutes, depending on temperature. For ingot microstructures deformed and held at very high temperatures, very quickly, after 10-20 seconds, metadynamic recrystallization has to rely only on the energy stored in sub-boundaries to progress, which is quite lower. It means that for multi-hit situations, increasing time between hits provides little benefit.

After free dislocations have been annihilated by recovery, when sub-boundaries provide the only driving force for recrystallization, a progressive decrease of recrystallization rate of the metadynamic regime of ingots is observed. Impingement of bubbles is partially responsible for that but it is not enough to explain it. This decrease is related to another geometric effect: the spatial distribution of sub-boundaries. The identified value of K_{absorb} is specified here, with a value of 0.6. It means that initial grains tend to have a repartition of sub-boundaries such that the actual value of sub-boundary density near recrystallized areas is about 60% higher than the average one over the whole grain volume. When these recrystallized areas grow, they consume the zones of high sub-boundary density first. And if new sub-boundaries are not generated, as in metadynamic regime, the more recrystallization progresses, the more the sub-boundary density is low. Thus the driving force decreases through geometric effects, which add to impingement effects already accounted for in the geometric framework (Figure III-6).

III.E.3. Sub-boundary and nucleation related equations

Sub-boundary generation is involved in two forms, depending on where the nuclei it may produce will be located. “Necklace” sub-boundary generation is given by equation (III-20), and in the volume, it is equation (III-21).

$$\dot{S}_{sb}^{+} = 4.6 * 10^{-6} \exp\left(\frac{133565}{RT}\right) \dot{\varepsilon} F\left(M_T\right) \exp\left(-\frac{D}{1500}\right) \qquad \text{(III-20)}$$

For a random set of crystallographic orientations, i.e. for wrought microstructures, M_T=3.06. This value was chosen as a reference to which other Taylor factor values are compared. As a result, F(3.06) was set to 1.

At $1s^{-1}$, for $F(M_T)$=1, and a grain size that tends towards 0, the necklace sub-boundary generation rate is 1.4 $\mu m^2/\mu m^3$ per deformation unit at 1000°C and 0.3 $\mu m^2/\mu m^3$ at 1177°C.

For the uniaxial compression of ingot microstructures oriented so that the main axis of columnar grains is transverse to the compression axis, M_T is about 3.1. It was chosen that F(3.1) would be equal to the one of a wrought microstructure, i.e. 1. For grains oriented parallel to the compression axis, M_T=2.45. F(2.45) was found to be 0.9. It means that axial grains tend to produce 10% less necklace sub-boundaries than average random or transverse orientations. For grains oriented at 45° of the compression axis, M_T is about 3.55. F(3.55) was found to be equal to 1 again. One can conclude that grain orientation has very little influence on the generation of necklace sub-boundaries.

Necklace sub-boundary generation decreases slowly as grain size increases, and so does the rate of nucleation too. But written by surface unit of grain boundary instead of by volume unit, the term of dependence with the grain size becomes D exp(-D/1500). It increases until about 1500µm and decreases slowly afterwards. The meaning of the initial increase is that the coarser the microstructure, the more it is difficult to adjust strain incompatibility between neighboring grains. Big grains tend to accumulate more geometrically necessary dislocations at their periphery, which induces a higher nucleation rate per surface unit of initial boundary, though the overall nucleation rate of the structure is lower. For very big

grains like ingot ones, one could have expected a simple stabilization of sub-boundary generation/nucleation rates at a high value. The obtained decrease is difficult to understand. Nevertheless, as grains get very coarse, strain incompatibility is more and more accommodated in the volume.

$$\dot{S}_{sbV}^{+} = 0.133 \exp\left(\frac{22135}{RT}\right) \dot{\varepsilon} F_V\left(M_T\right) \qquad \text{(III-21)}$$

As for necklace sub-boundary, the Taylor factor of a randomly oriented microstructure was used as the reference for volume sub-boundary generation, and transverse ingot grains in uniaxial compression where supposed to behave similarly. So $F_V(3.06)=F_V(3.1)=1$.

At $1s^{-1}$, for $F_V(M_T)=1$, the volume sub-boundary generation rate is 1.1 $\mu m^2/\mu m^3$ per deformation unit at 1000°C and 0.85 $\mu m^2/\mu m^3$ at 1177°C.

For axial grains, $F_V(2.45)$ was found identical to the one of transverse grains, i.e. 1. For grains oriented at 45°, it was found to be $F_V(3.55)=1.1$: 10% more volume sub-boundary are generated in average for 45° grains. It may look surprising to see, here again, so low dependence of sub-boundary generation with the orientation. However, observed metadynamic recrystallization rates are not so different from an orientation to another. And it has to be reminded that after few tens of seconds of holding time, because of metadynamic recovery, only sub-boundaries provide the driving force for metadynamic recrystallization. Thus sub-boundaries had to be generated in similar quantities. The investigation of critical strains, and related disorientation rates, reveals where crystallographic orientation has the largest influence.

The critical strain for necklace nucleation is given by equation (III-22), and in the volume, it is equation (III-23).

$$\varepsilon_c = 0.05 F_c\left(M_T\right) \qquad \text{(III-22)}$$

No dependence of necklace critical strain could be identified with temperature. On the contrary, its dependence with grain orientation is very strong. Once again, average behavior of a randomly oriented microstructure is the reference, as the one of transverse grains, so $F_C(3.06)=F_C(3.1)=1$. For grains oriented at 45°, $F_C(3.55)$ was found to be 0.9, i.e. the disorientation rate is about 10% higher. For axial grains, $F_C(2.45)$ was found to be dramatically larger with a value of 2.5. It means that the disorientation rate of necklace sub-boundaries is 2.5 times slower than for other cases. Sub-boundaries are generated in similar quantities, but they tend to delay considerably their conversion into high angle boundaries. We attribute such behavior to the fact that axial grains have not only a low Taylor factor but also the same for all of them and, most important, to the stability of their orientation in uniaxial compression. The two latter items must limit strain heterogeneity a lot, whereas it is a necessary condition to accumulate geometrically necessary dislocations in sub-boundaries, and initiate nucleation.

$$\varepsilon_{cV} = 0.0236 \exp\left(\frac{26892}{RT}\right) F_{cV}\left(M_T\right) \qquad \text{(III-23)}$$

Little dependence with temperature of the critical strain for volume nucleation was found. For $F_{CV}(M_T)=1$, i.e. for wrought and transverse ingots microstructures, it varies form 0.3 at 1000°C to 0.22 at 1177°C. These values are greater than those of necklace nucleation. It shows that second phase particles do not have as strong effect on disorientation as (initial) grain boundaries. As noticed in the case of necklace critical strain, for grains oriented at 45°, $F_{CV}(3.55)$ is about 0.9, i.e. it gives a 10% higher disorientation rate. But for axial grains, once again, the critical strain is much higher, by a similar value $F_{CV}(2.45)=2$. Clearly here, the disorientation delay is related to the stability of deformation of axial grains. Second phase particles which are supposed to induce a spread of crystallographic orientations cannot play that role probably because the slightly different deformation tensor they induce in their neighborhood is not able to spread orientations away from the <100> fiber. The delay of nucleation cannot be due to

an energy criterion because metadynamic recrystallization rate of axial grains is almost the same as the one observed for the two other orientations (transverse and 45°), which shows that stored energies are actually very similar.

At every instant during deformation, once critical strain is reached (x=1 or x_V=1), nucleation starts. A fraction of sub-boundaries tends to become high angle boundaries that delimit nuclei. The rate of conversion for necklace nucleation is given by equation (III-24) and in the volume it is equation (III-25).

$$\dot{S}_{sb}^{-} = \dot{S}_{b}^{+} = 1.0\ \dot{\varepsilon}\left(x-1\right)S_{sb} \tag{III-24}$$

$$\dot{S}_{sbV}^{-} = \dot{S}_{bV}^{+} = \left(0.01+75\ S_B^2\right)\dot{\varepsilon}\ \left(x-1\right)S_{sbV} \tag{III-25}$$

The coefficients that define the conversion rates are related to the number of sites where sub-boundaries of high disorientation may become grain boundaries. As long as bubbles of recrystallized grains have not developed around second phase particles, the density of zones potentially affected by volume nucleation is very low. It is just the areas surrounding second phase particles. Thus the conversion rate was found to be about two orders magnitude lower than the one found for necklace nucleation, which can rely on existing high angle boundaries and on their role of site of accommodation of strain incompatibility. But when bubbles of recrystallized grains develop, the areas affected by volume nucleation get larger. They could have been expected to be just proportional to the surface of bubbles in grains, but it is actually more than that, as a square relationship was found to be necessary. It is possible that not only the surface of bubbles itself increases the density of sites, but also that, as bubbles grow, they induce a larger perturbation of the strain distribution inside the grains, which may accelerate sub-boundary conversion too.

Finally, the nuclei size is given by equation (III-26).

$$D_N = 1115 \exp\left(-\frac{53674}{RT}\right) \quad \text{(III-26)}$$

It provides nuclei of 7µm at 1000°C, and 13µm at 1177°C. Dependence with the strain rate could be added to provide a more realistic behavior in some situations. However, such an addition does not induce a noticeably lower average error of the model, while it increases the number of parameters to adjust. The goal is to represent only dependencies that were absolutely necessary to reach an average error of the model below 10%.

Conclusion

A meso-scale mechanism-based model of recrystallization was developed. It relies on two main parts: a geometric framework and a set of differential equations that represent driving forces. The geometric framework is based on MesoStructure Units (MSUs) that can be seen as aggregates of grains of similar properties and behavior. MSUs are the elementary bricks used to perform the geometric description of microstructures. From a set of geometric assumptions, mainly related to grain locations and shapes, a set of laws is obtained. Its role is to insure that the geometric description remains meaningful through mechanisms that affect grain geometric variables, i.e. nucleation and grain growth. The combination of the geometric description and of these laws constitutes the geometric framework. For instance, the geometric framework insures volume conservation naturally. It responds to two types of input: the grain boundary velocity of each pair of MSUs, and the nucleation rates produced by each MSU. These two inputs are provided by equations that represent driving forces. These equations can be separated in three groups, which correspond to the discontinuous dynamic recrystallization main sequence: energy storage, nucleation and grain growth (boundary migration). Energy storage equations define the evolution of dislocation densities, with strain hardening and recovery. One could add to this group sub-boundary generation equations, though they belong to the second group too. This group connects sub-structure evolution with nucleation. Sub-boundary disorientation equations induce disorientation variables to reach their critical value. Then, equations that represent the conversion of some sub-boundaries into grain boundaries are used to obtain the nucleation rate. Finally, for the third group, grain growth and boundary migration rely on a grain boundary mobility equation and on equations that define the pressure seen by the grain boundaries during the various kinds of interactions taken in charge by the geometric framework.

The model was implemented in RX-MOD, software dedicated to the treatment of such models of microstructural evolution, in order to be applied to Waspaloy, for which a lot of experimental data was available, for wrought microstructures and ingot ones. The latter include an investigation of grain orientation effects, which was shown to have great influence on recrystallization rates, especially during the dynamic regime.

The model could be solved to reach an average error on recrystallized fractions below 10%. However, average error depends on the type of data. Wrought microstructures in dynamic and metadynamic regimes, and ingot ones in the dynamic one, exhibit the best precision, with about 7.5% average error. But taking into account the metadynamic regime observed on ingots increases the discrepancy. We think that it is mostly related to the size of characterized zones, which makes measurements very sensitive to the local Taylor factor. The model reveals that, for ingot microstructures, most of the grain orientation dependence lies in sub-boundary disorientation kinetics, especially for so-called axial grains, i.e. grains whose <100> axis is parallel to the compression axis. For these, very much lower disorientation kinetics was necessary to represent the required delay of nucleation. It was attributed to the stability of the <100> fiber during uniaxial compression. The ingot metadynamic regime precision is the best for axial grains, a bit worse for transverse grains, and looks bad for 45° grains. This is to be related to the range of Taylor factors present in the structure, as one can see that the larger the range of Taylor factors, the higher the discrepancy of measured data. For axial grains, which all have the same Taylor factor in uniaxial compression, the discrepancy was the lowest and the model exhibits an acceptable behavior for instance. To reach observed local variations, a calculation made on extreme Taylor factor values can be considered for future investigations, in order to evaluate the discrepancy of recrystallized fractions to expect.

Though they provide interesting insight on the involved mechanisms, sub-boundary and nucleation equations are still empirical. One could for instance wonder if the

conversion rates should not carry some orientation dependence. Dependence of sub-boundary generation with the strain rate may look appropriate. But none of them really improves the model response in terms of overall error. However, deeper re-formulation could help reducing the number of parameters, obtain more meaningful expressions and re-connect comparable behaviors. Strong similarities between necklace and volume sub-boundary parameters tend to push in that direction. In addition, once bubbles of recrystallized grains have percolated and they isolate the remnants of initial grains from their neighbors, it may be possible to deal with these remnants just like regular grains from a wrought microstructure. Such consideration puts the focus on the links between necklace and volume sub-boundaries, as the latter would have to be considered suddenly like necklace ones. Required continuity of the model through this operation may impose some constrains or help understanding better the dependence of the conversion rate of volume sub-boundaries with the surface of bubbles.

In terms of extension of the model to other superalloys, with minimum amount of tests and characterized microstructures, it is quite probable that crystallographic orientation influences should not be too different. They are low in most cases. And the very special behavior of axial columnar grains identified on Waspaloy would at least provide an interesting first guess. But the variation of sub-boundary generation rates from an alloy to another is difficult to predict, given the still empirical character of sub-structure evolution equations at this stage of development. Grain boundary mobility equation parameters need only few tests of grain growth of a fine recrystallized microstructure – after a strong deformation for instance – to be identified. Strain hardening and recovery are not expected to change too much, since the shape of stress-strain curves does not change very much either. Similarities will appear through an increase of the number of alloys treated with this modeling method, and one can expect that each new alloy added will help reducing investigations for the next ones.

It is important to realize how different this model adjustment is different from an Avrami-based one. Most values of driving forces at extreme temperatures of the tested domain could be set almost as round ones, which shows that the most important is their order of magnitude more than their actual value. It means that, contrarily to an Avrami-based model, the response of the model is not given so much by parameters that can change dramatically the shape of the Avrami curves, but by its deep structure and inner interactions. The orders of magnitude of parameters, since almost all of them represent some physical meaning, will not change dramatically from an alloy to another, at least of close compositions. Though at this stage of development it may be difficult to guess which parameters will need to be modified and how, this modeling method is very promising to progressively reduce thermomechanical testing in the future.

The model was implemented to be applied on 2D and 3D FEM calculations. Only 2D calculations have been tested yet (Figure III-7). 3D cases will bring questions about actual average Taylor factors to use in the case of complex deformation tensors, and about interpolation of Taylor-factor-dependant functions for which only discreet values where investigated.

References

[1] D. Zhao, C. Cheng, R. Anbajagane, H. Dong and F.S. Suarez, Superalloys 718, 625, 706 and various derivatives, Ed E.A. Loria, TMS, 1997, pp 163-172

[2] G. Shen, S.L. Semiatin and R. Shivpuri, Metal. Mater. Trans., 1995, vol. 26A, pp 1795-1803

[3] F. Montheillet, Proc. of the 4th Int. Conf. on Recrystallization and related phenomena, 1999, pp 651-658

[4] Thomas

[5] S.L. Semiatin, D.S. Weaver, P.N. Fagin, M.G. Glavicic, R.L. Goetz, N.D. Frey, R.C. Kramb and M.M. Anthony, Metal. Mater. Trans., 2004, vol. 35A, pp 679-693

[6] A. Di Shino and G. Abbruzese, Proc. of the 1st joint int. conf. on recrystallization and grain growth, 2001, pp 1021-1026

[7] F.J. Humphreys, Scripta Mater., 2000, vol. 43, pp 591-596

[8] A. Laasraoui and JJ. Jonas, Acta Mater., 1991, vol. 47, pp 4695-4710,

[9] B. Marty, J.Y. Guedou, P. Gergaud and J.L. Lebrun, Superalloys 718, 625, 706 and various derivatives, Ed. E.A. Loria, TMS, 1997, pp 331-342

[10] J.C. Glez and J. Driver, Acta Mat., 2003, vol. 51, pp 2989-3003

[11] L.E. Murr, Interfacial phenomena in metals and alloys, Addison-Wesley Publishing Company, 1975

[12] A.P. Zhilyaev, G.V. Nurislamova, S. Surinach, M.D. Baro and T.G. Langdon, Mater. Phys. Mech., 2002, vol. 5, pp 23-30

[13] M. Zhou and M.P. Clode, Computational Materials Science, 1998, vol. 9, pp 411-419

Figures

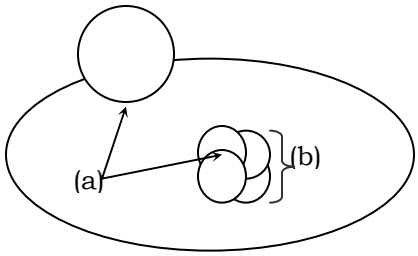

Figure I-1: (a) Envelope-envelope and (b) bubble-envelope interactions

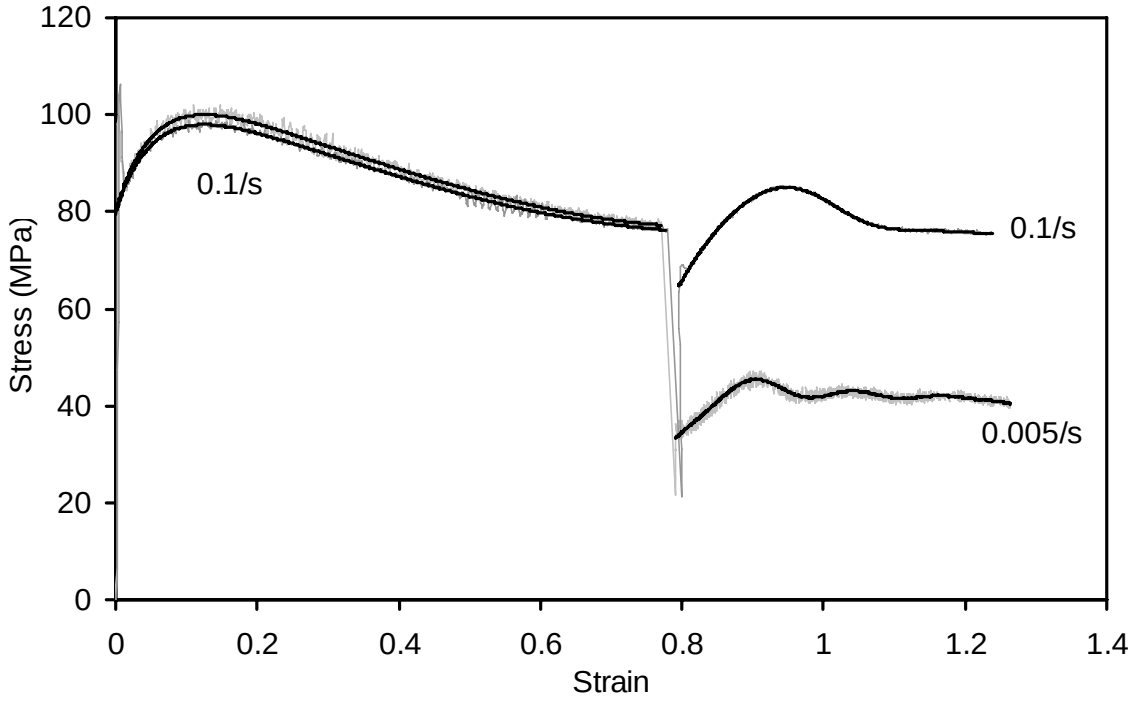

Figure II-1: Double-hits performed at 1177°C on wrought Waspaloy

with a 3 second holding time between hits

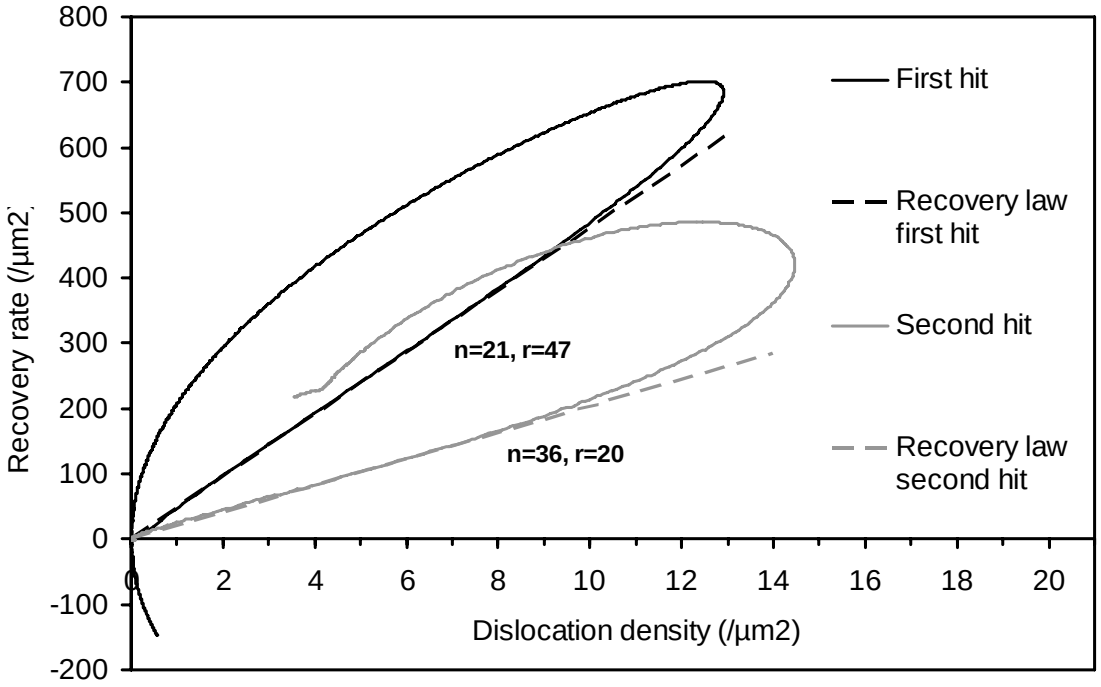

Figure II-2: Apparent recovery rate on a double-hit performed at 1177°C and 0.1s^{-1} on wrought Waspaloy with a 3 second holding time between hits

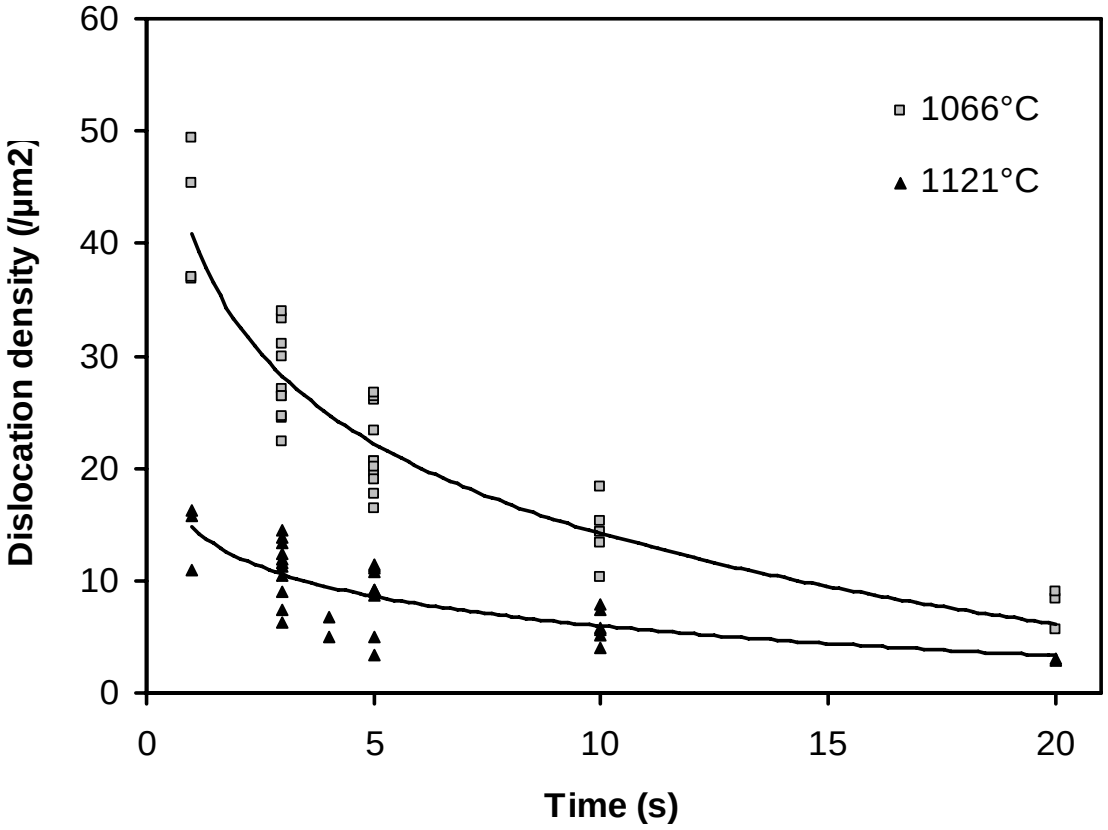

Figure III-1: Dislocation densities deduced from metadynamic recrystallization rates of an Avrami formulation and estimation of grain boundary mobility

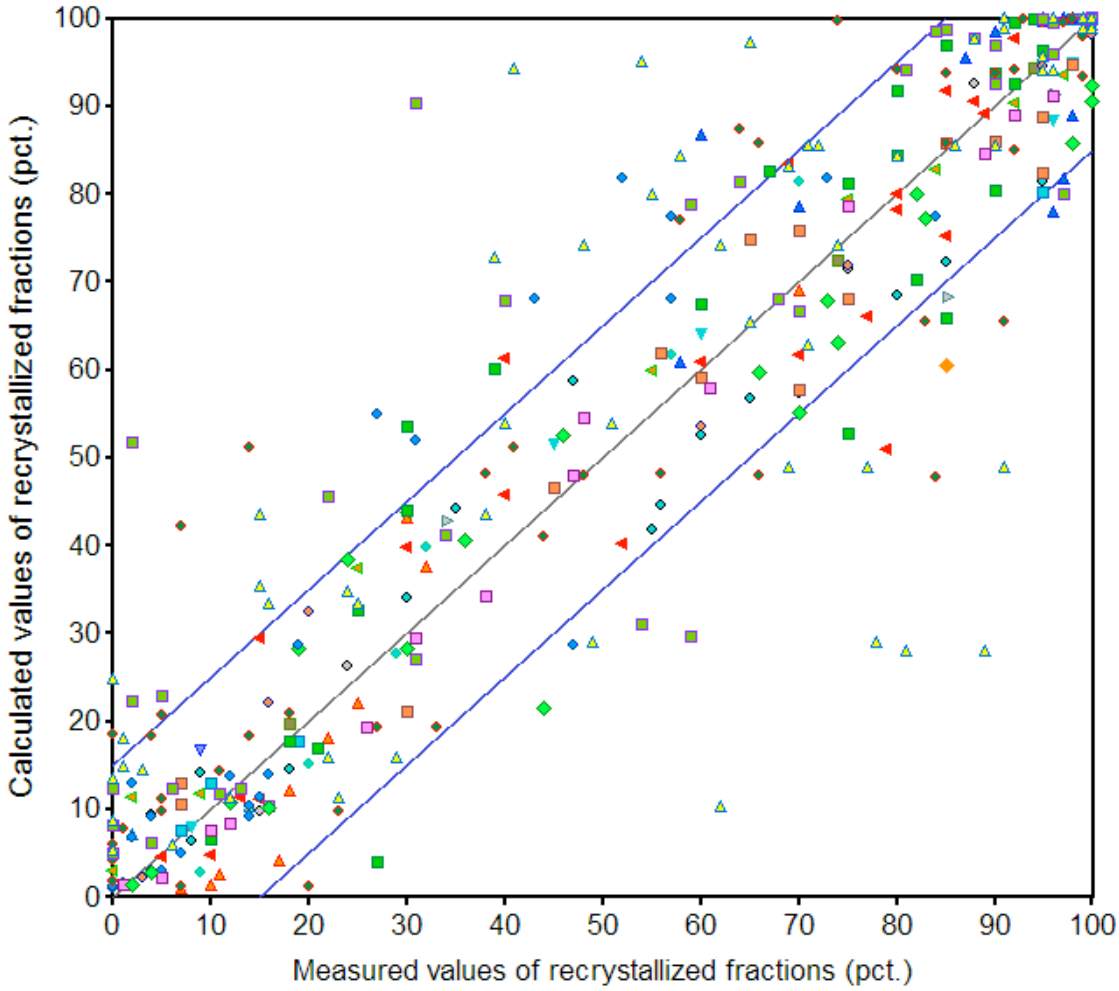

Figures III-3-b: error graphs with values of dynamic and metadynamic recrystallized fractions of wrought and ingot microstructures

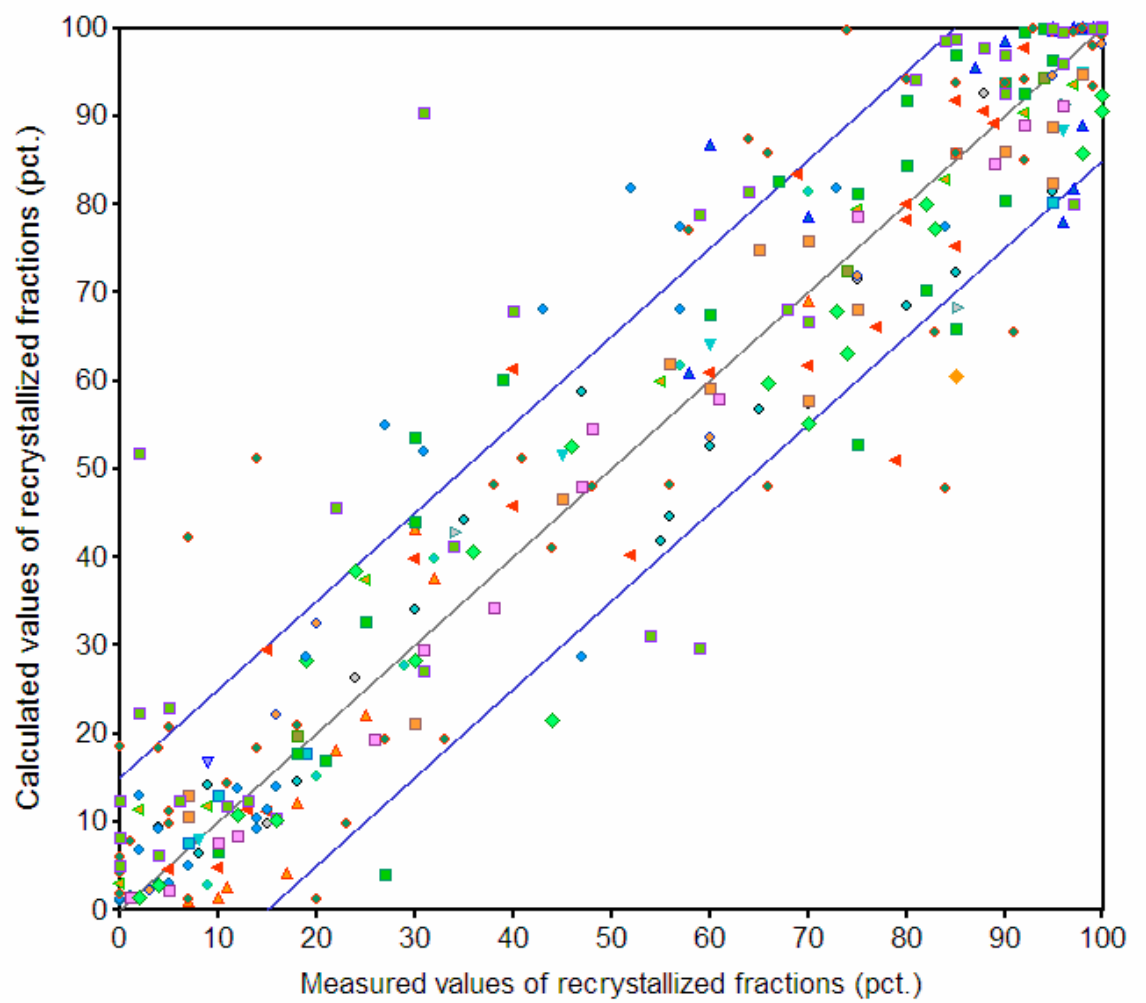

Figures III-3-b: error graphs with values of dynamic and metadynamic recrystallized fractions of wrought microstructures, dynamic values of ingots microstructures, and metadynamic values of axial and transverse ingot microstructures

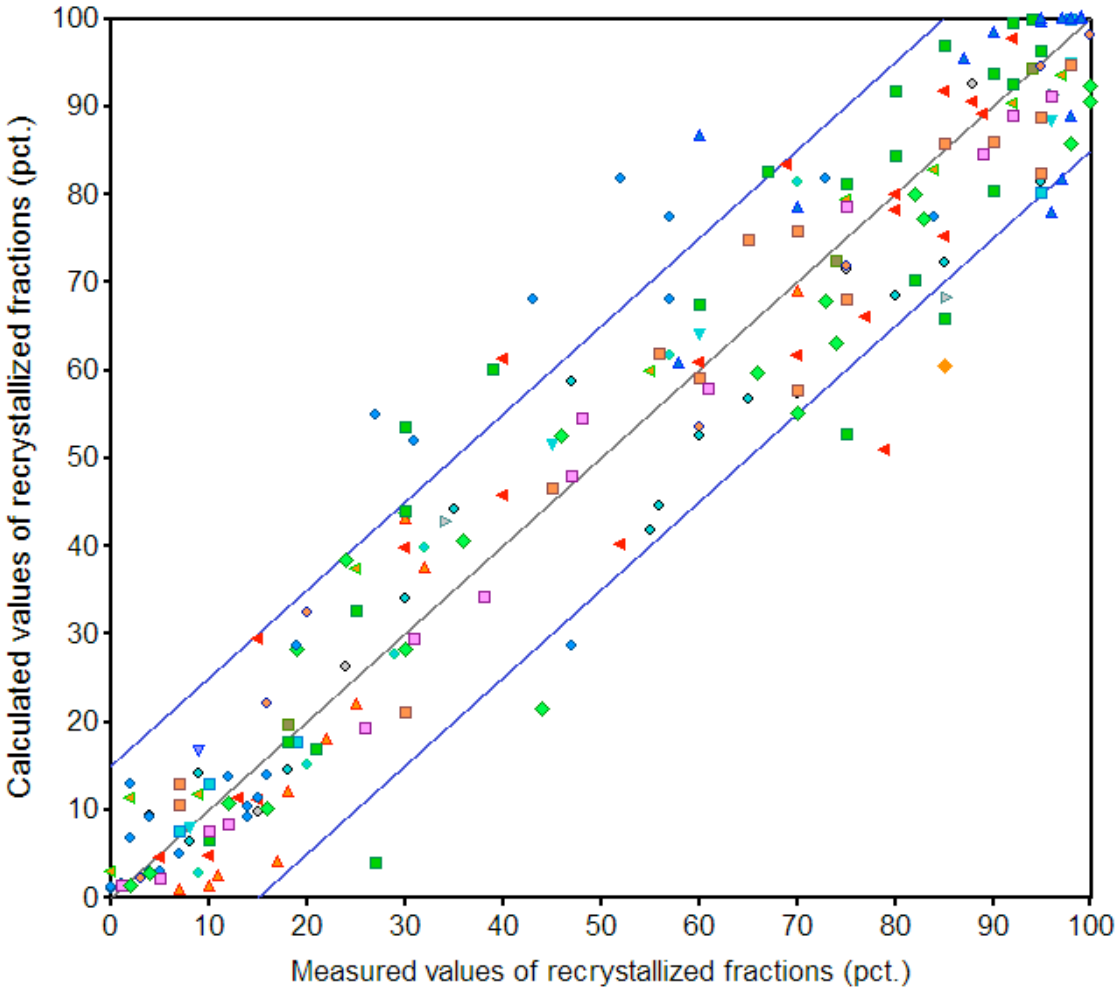

Figures III-3-c: error graphs with values of dynamic and metadynamic recrystallized fractions of wrought microstructures and dynamic values of ingots microstructures

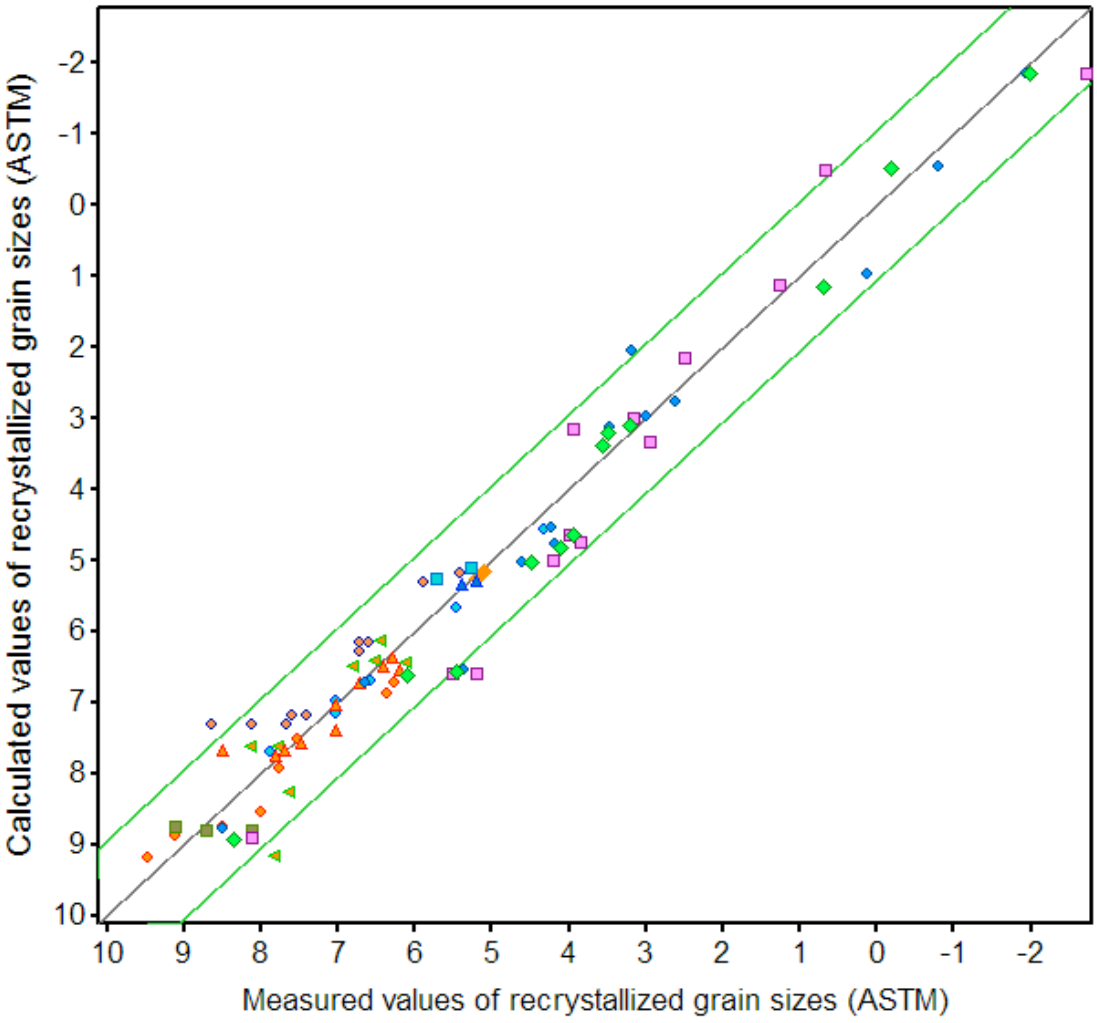

Figure III-4: error graph for grain sizes – average error: 13% i.e. about half an ASTM

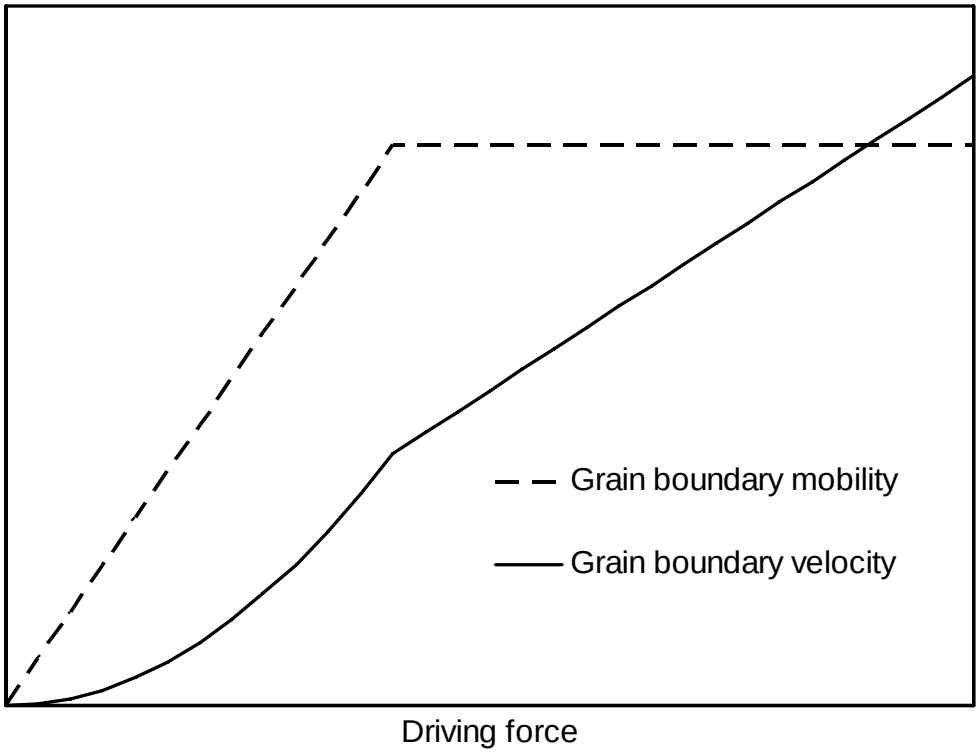

Figure III-5: Grain boundary mobility with saturation value and grain boundary velocity in arbitrary units

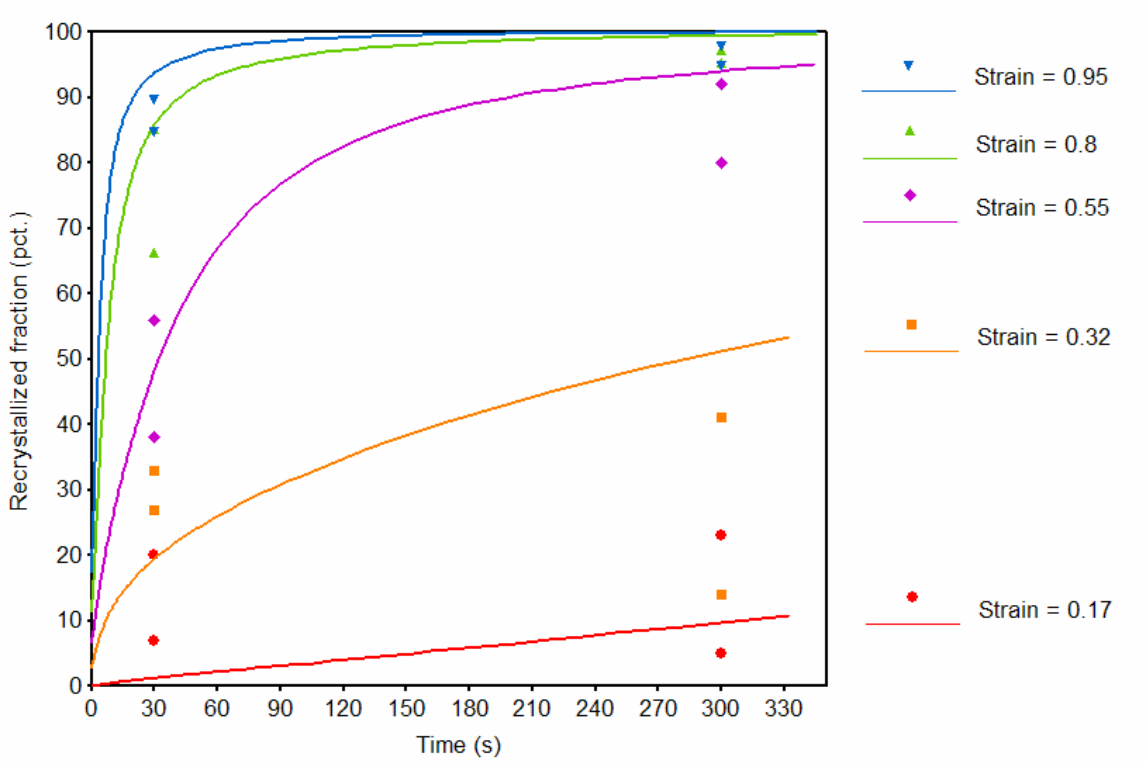

Figure III-6: Metadynamic recrystallized fractions of axial ingot deformed at 1177°C

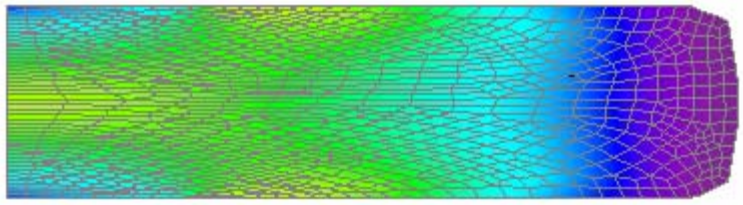

Figure III-7: Map of recrystallized fraction in a double-cone